Journal of Superconductivity and Novel Magnetism (2019) 32:23–44
https://doi.org/10.1007/s10948-018-4884-4

ORIGINAL PAPER

Superconductor Electronics: Status and Outlook

Alex I. Braginski[1]

Received: 10 September 2018 / Accepted: 17 September 2018 / Published online: 16 November 2018

Abstract

Superconductor electronics combines passive and active superconducting components and sometimes normal resistors into functional circuits and systems that also include room-temperature electronics for amplification, power sources, necessary controls, etc., usually computer operated. Furthermore, complete systems include magnetic and electromagnetic shielding, cryogenic enclosures, and increasingly a cryocooler in self-contained units. Components or devices of low or high critical temperature superconductors include inductances (coils), passive transmission lines, resonators, antennae, filters, as well as active elements: Josephson junctions, Josephson oscillators, and superconducting quantum interference devices. Of multiple demonstrated applications, mostly but not only in science and metrology, currently most successful are voltage standards, astronomy detectors and large telescope cameras, instruments for material characterization, and magnetometers for geomagnetic prospecting. Major current efforts concentrate on energy-efficient high-end computing and quantum computing. The outcomes of these efforts are likely to be known in the course of the following decade.

Keywords Superconductor electronics · Flux quantum · Transmission line · Resonator · Josephson junction · Josephson oscillator · SQUID · SQUID magnetometer · Astronomy detector · Multiplexer · Single flux quantum logic · SFQ: rapid SFQ · RSFQ · Energy-efficient SFQ · ERSFQ · Reciprocal quantum logic · RQL · Adiabatic quantum flux parametron · AQFP · Qubit · Transmon · Quantum processor · Quantum computing · Adiabatic annealing

1 Introduction

Superconductor electronics (SCE) are functional electronic circuits incorporating active (nonlinear) and passive (linear) elements that are superconducting below the critical temperature (T_c). Normal conducting resistors may be included, if functionally necessary. In applications and when operated sufficiently below T_c, such circuits may exhibit unique characteristics and unsurpassed performance not attainable by conventional semiconductor electronics. However, the necessity of cooling to and operating at cryogenic temperatures is the main penalty that severely limits practical uses and thus far constrains SCE to remain a niche technology. It is and will be used only when nothing else will do or when operation at very low temperatures is necessary for quantum performance, independent of the device and circuit technology applied.

This short overview refrains from tutorial descriptions and most technical details; given are only few examples. I attempt instead to briefly characterize the status of devices, circuits, and their practical applications, including my views on the possible future developments. Fundamentals of SCE are given in [1, 2]. My earlier overview of SCE dates back to 1996/1997 and could still include many examples [3]. Thanks to the impressive development of this field, now I attempt mostly to highlight the progress of the last two decades in what amounts to little more than a topical guide to the SCE abundant literature. I should note that a recent handbook on superconductor devices and applications devotes about 400 pages to a relatively up-to-date coverage of SCE [4].

Superconductor electronics exploit basic properties of superconductors such as the magnetic flux exclusion (the Meissner effect), flux quantization, extremely low absorption (power dissipation) in AC fields up to the gap frequency (f_g), and both DC and AC Josephson effects with related macroscopic quantum behavior. For SCE, the

The original version of this article was revised: The acronyms for conventional Josephson voltage standard (CJVS) and programmable Josephson voltage standard (PJVS) were misspelled as CVJC, PJVC and PVJC.

✉ Alex I. Braginski
a.braginski@fz-juelich.de

[1] Institute of Complex Systems (ICS-8), Forschungszentrum Jülich (FZJ, Research Center Juelich), D-52425 Juelich, Germany

superconductor material workhorse is niobium (Nb), having $T_c \approx 9$ K and $f_g \approx 0.7$ THz. It is a conventional (s band) low-temperature superconductor (LTS) suitable for circuit operation typically at 4 to 5 K. Other LTSs, with much lower T_c, are widely used in radiation and particle detectors and in quantum bits (qubits). Conventional superconductors with T_c higher than that of Nb, such as niobium nitrides, carbonitrides and MgB_2 are rarely used, although the latter may have some future in applications.

In spite of their T_c and f_g, an order of magnitude higher than in the case of Nb, the unconventional (d band) superconductors (HTS materials), typically represented by rare-earth cuprates such as $YBa_2Cu_3O_{7-\delta}$ (YBCO), found thus far only limited use in electronics, mostly in passive devices such as high-frequency resonators and filters and in portable magnetometers. This is due primarily to the difficult, expensive, and less-reliable fabrication technology of epitaxial films and multilayers necessitated by the extremely short coherence lengths, high anisotropy of properties and, caused by thermal energy, inferior performance at higher temperatures, typically at or around that of liquid nitrogen (LN_2). Low price and wide availability of this coolant, as well as much higher efficiency and reliability of cryocoolers used in this temperature range, did not outweigh thus far the disadvantages indicated above, except in mobile applications, such as minerals exploration, for example.

In SCE components, devices, and circuits, superconductor thin films are incorporated into multilayered patterned structures together with other thin film materials, primarily insulators and normal conductors (e.g., for resistors and contact metallization) on suitable low dielectric permittivity (ε) and loss ($\tan\delta$) substrates such as Si, quartz, glass, and sapphire in the case of LTS electronics. Of insulators, most typical are SiO_2, SiO, Al_2O_3, and anodized Nb. The HTS electronics requires epitaxial films and lattice-matching substrates such as $SrTiO_3$ for low-frequency circuits, MgO, $LiNbO_3$, and similar perovskites for high-frequency (HF) applications. The integrated circuit (IC) fabrication is largely analogous to that of semiconductors while much less advanced than the latter. Nanotechnology and large-scale integration (LSI) needs, driven mostly by current efforts into digital SCE development, thus far resulted in demonstrated integration levels approaching 10^6 functional devices on the chip, with 10^4 being typical in existing applications. The IC fabrication with eight to ten photolithography-patterned levels represents the current state of the art and is practiced mostly in commercial and laboratory foundries of which currently most advanced are those operated by D-Wave and MIT Lincoln Labs (LL) in the USA and the National Institute of Advanced Industrial Science and Technology (AIST, located in Tsukuba, Ibaraki) in Japan.

The basic linear components and devices in superconductor circuits are low-loss transmission lines, antennae, high-quality-factor (Q) resonators, and filters. The most basic nonlinear two-terminal device with unique properties is the Josephson junction. The superconducting quantum interference devices (SQUIDs) incorporating JJs are also components of many electronic circuits.

Each practical SCE electronics system consists of the following essential building blocks: (1) the SCE device circuitry, (2) magnetic and electromagnetic shielding of that circuitry, (3) cryogenics assuring the very low and stable operating temperature (or selected temperature levels), and (4) the room temperature electronics for readout and control including the necessary power supply with various biasing sources. (5) In mobile systems, motion and vibration compensation measures are usually required. Below, the first three are briefly addressed.

2 Building Blocks

2.1 Passive Superconductor Devices

Linear devices are best characterized by the frequency dependence of the superconductor surface impedance (Z_s). Its real (loss) part is the surface resistance (R_s), the imaginary part is the kinetic inductance. At frequencies with photon energies sufficiently below that of energy gap (f_g) and below T_c, these losses are orders of magnitude lower than in a cooled normal conductor such as high-purity copper at the same T. For reasons probably related to d-wave symmetry, the losses in HTS are somewhat higher than in niobium at the same reduced temperature $(t_r) = T/T_c$ and frequency $(f_r) = f/f_g$, but still low enough. At microwave frequencies, the practical consequence of the low superconductor losses, and of the fact that $\tan\delta$ of crystalline substrates decreases rapidly with T, are low-loss transmission lines and high-quality factor (Q) resonators. For thin film planar (microstrip, stripline, coplanar, or lumped element) HTS resonator, Q values between 10^3 and 10^5 are readily obtainable at 77 K and mostly HTS resonators are used today, although novel applications emerge for LTS resonators. Three-dimensional dielectric resonators shielded with HTS films attain 10^5 to 10^7 in low-intensity electromagnetic fields. In higher radiofrequency (RF) fields, when the RF current exceeds its critical value, losses increase dramatically and nonlinear effects appear. Similarly, transmission lines exhibit extremely low insertion losses and are nondispersive, i.e., their phase velocity remains frequency-independent up to f_g. Fundamentals of resonators and transmission lines can be found in textbooks on microwave engineering, for example [5].

2.2 Active Superconductor Devices

The essential superconductor nonlinear devices are the Josephson junctions (JJs) and SQUIDs. Both exhibit rich quantum physics at a macroscopic scale and have no equivalents in semiconductor electronics. Theory and properties of JJs are systematically presented in textbooks [1, 2]. Other two textbooks [6–8] cover SQUIDs and their applications in considerable detail, but are somewhat dated, especially with respect to applications. More up to date on these is [4]. The theory and experiments elucidating macroscopic quantum properties of JJs are reviewed and summarized in [9].

The term Josephson junction encompasses all two-terminal devices having two superconducting electrodes with a weak link connecting these, whether an insulating tunnel barrier for Cooper pairs, a point contact, planar micro/nanobridge (Dayem bridge), or a proximity link. The behavior of a Josephson junction is described by the two Josephson equations:

$$I = I_0 \sin\varphi \tag{1}$$

$$\partial\varphi/\partial t = 4\pi V e/h = 2\pi V/\Phi_0 \tag{2}$$

The supercurrent I through a JJ is given by the 1st equation, where I_0 is the junction's critical current and φ is the difference $\varphi_1 - \varphi_2$ between phases of the superconductor's function of state in two weakly linked superconducting electrodes. Equation (1) defines the static properties of a JJ. At currents exceeding I_0, voltage drop (V) appears across the JJ and phases of the functions of state are slipping relative to each other at a rate determined by (2), where e is the electron charge, h the Planck constant, and Φ_0 the flux quantum. Hence, in the voltage state, the JJ emits radiation of frequency $f_J = 2eV/h \approx 483\ V$ (MHz/μV) and the correlation between V and f_J is defined only by fundamental constants. The idea of V-tunable oscillators has been intensely pursued experimentally but without convincing technical success for LTS.[1] When a voltage-biased JJ is exposed to an external rf (microwave) field of frequency (f), its $I-V$ characteristic exhibits sharp current steps, the so-called Shapiro steps, at voltages $V = nhf/2e$, where $n = 0, 1, 2, 3$ ... is an integer.[2]

Practical JJ devices are planar, single layer, or multilayer structures fabricated of thin films, and most widely used

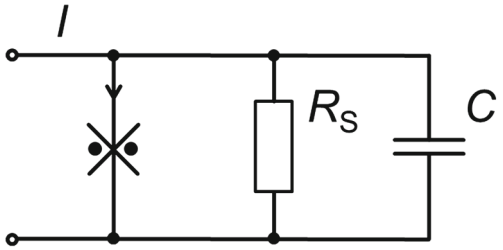

Fig. 1 Equivalent circuit of current-biased Josephson junction. From left to right, the new symbol of Josephson junction behavior, effective shunt resistance of the junction, $R_s = R_n R/(R + R_n)$ where R is junction's internal resistance and R_n is the resistance of an external shunt resistor

are superconductor-insulator-superconductor (SIS) trilayer JJs fabricated in Nb/AlO_x/Nb technology. Their behavior is adequately described by the equivalent circuit of Fig. 1, which includes the capacitance between electrodes C and the shunting normal resistance R of the weak link itself, very high for SIS devices. The unfamiliar graphic symbol to the left represents the Josephson characteristics according to the new standards of IEC.[3] Due to C, static $I - V$ characteristics are hysteretic or undamped, when R is very high, typical for tunnel junctions. Once $I > I_0$, the undamped JJ switches into the voltage state and remains in it even when the bias voltage drops below the gap voltage (V_g), as shown in Fig. 2a. In this case, to eliminate hysteresis, an external shunt R_n is required. Damping of shunted JJs is characterized by the Stewart-McCumber parameter β_c:

$$\beta_c = 4\pi(e/h) I_0 R_s^2 C,\ R_s = R_n R/(R_n + R). \tag{3}$$

when $\beta_c \leq 1$ hysteretic behavior is not observed, i.e., the junction is damped. Known HTS junctions are usually internally damped, no R_n is needed. Recently, internally damped LTS junctions have also been developed (see Section 7), and interest in their technology is growing. A novel class of low-T_c JJs are those with magnetic barriers (see Section 8.3). Their physics is most interesting, but they cannot be highlighted here.

[1] Best to date has been the demonstration of THz oscillators in intrinsic HTS JJ stacks of BSCCO, with output power limited by internal heating effect.

[2] Note that (1) and (2) describe only the Cooper pair supercurrent. When $V > 0$ and $T > 0$, a quasiparticle current component appears.

[3] International Electrotechnical Commission: IEC 61788-22-1 standard on "Superconductivity—part 22-1: superconducting electronic devices—generic specification for sensors and detectors": https://webstore.iec.ch/publication/26674; IEC 60617—graphical symbols for diagrams: superconducting region, one superconducting connection (S01924), normal-superconducting boundary (S01925), and Josephson junction (S01926), https://webstore.iec.ch/publication/2723. Free access: http://snf.ieeecsc.org/sites/ieeecsc.org/files/documents/snf/abstracts/edOhkuboM_Report_of_IEC-IEEE_joint_std_IWSSD20160129-final-4_040617.pdf

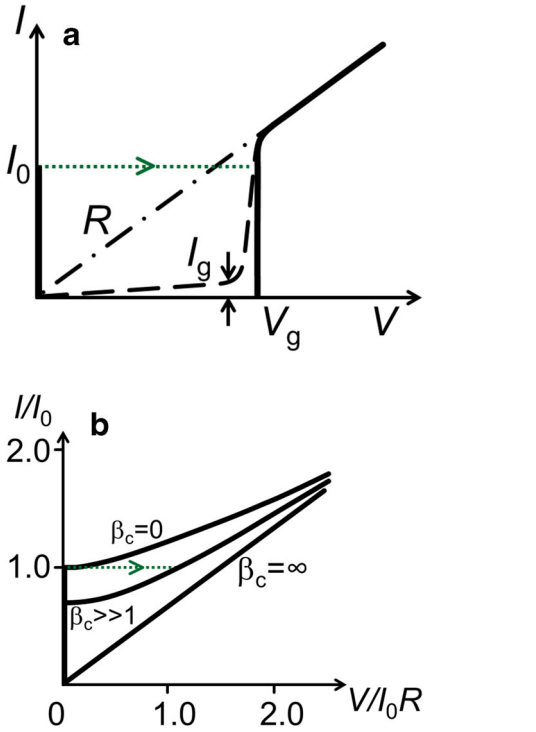

Fig. 2 **a** Idealized $I - V$ characteristic of undamped Josephson junction: I_0, JJ critical current; V_g, gap voltage; I_g, subgap or leakage current; R, JJ internal resistance. The dotted horizontal line symbolizes the jump to voltage state at I_0. **b** Idealized and superposed $I - V$ characteristics of damped JJs at three values of β_c indicated in the graph. The dotted horizontal line symbolizes the jump to voltage state of the JJ having $\beta_c >> 1$

In external magnetic fields B, when magnetic flux Φ is threading a JJ the $I_0(\Phi)$ dependence is given by (4), which describes the diffraction (Fraunhofer) pattern with period Φ_0:

$$I_0(\Phi) = I_0|\sin(\pi\Phi/\Phi_0)/(\pi\Phi/\Phi_0)| \quad (4)$$

Here, $\Phi_0 = h/2e = 2.0679 \times 10^{-15}$ Wb is the flux quantum, h the Planck's constant and e the electron charge. The cursory description above shows that JJs are not simply superconducting analogs of semiconductor diodes, just having the energy gap orders of magnitude lower than semiconductors.

Everything said thus far about JJs applies only to devices which are small compared with the Josephson penetration depth (λ_J). In undamped JJs much longer than λ_J, the magnetic self-field penetrates the barrier and electrodes as flux quanta (fluxons) with associated screening currents called Josephson vortices, which behave as (quasi)-solitons. This is shown schematically in Fig. 3. In external B, fluxons move with phase velocity of electromagnetic wave in the composite medium of thickness (Λ) shown in Fig. 3, the sum of barrier thickness (d) plus the double London penetration depth ($2\lambda_L$) of electrodes. This (Swihart)

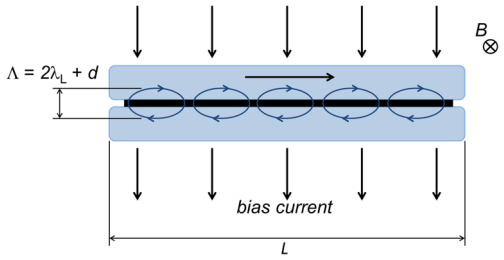

Fig. 3 Idealized cross-section of a long JJ of length (L) uniformly biased by current (symbolized by vertical arrows) and magnetic field B. The thick horizontal line represents the tunneling barrier separating two JJ electrodes. The row of circles symbolizes Josephson fluxons/vortices moving in the direction indicated by the horizontal arrow. Symbol Λ indicates the thickness of the composite medium in which the motion occurs with λ_L-London penetration depth (λ_L) and spacing between the JJ electrodes (d)

velocity, typically a few percent of the speed of light (c), results in emission of radiation, which for practical B values falls into centimeter to submillimeter wavelength range. Consequently, long JJ oscillators are feasible, see Section 4.2.

In contrast to semiconductor electronics, a single-element three-terminal device fully analogous to a transistor in being capable of power gain and fan-out does not exist. Devices with either current or voltage gain are possible. However, SQUIDs can be considered to be three-terminal devices, with the gate signal being the electromagnetic (EM) field threading the loop. SQUIDs are capable of power amplification up to RF frequencies in gigahertz range. Properties and characteristics of devices and circuits incorporating DC SQUIDs are addressed in conjunction with their various applications.

The most widely used DC SQUID incorporates two JJs interrupting a closed superconducting loop biased by external current or voltage source. The RF SQUID includes only one JJ and in most cases is inductively RF biased via a resonant tank circuit. SQUIDs with more than two JJs are used as some types of qubits. The general property of any SQUID is that, when biased into the voltage state, its output signal (voltage or current) is a periodical function of the magnetic flux threading the SQUID loop, with the period equal Φ_0. In the following sections, only DC SQUIDs are covered while RF SQUIDs are described in [10].

2.3 Shielding

Magnetic field and flux vortices, mostly of Abrikosov type, as well as electromagnetic fields, can penetrate superconducting films and devices in several ways. Static (DC) field biasing causes changes in operating parameters, electromagnetic interference (EMI), electromagnetic crosstalk, low-frequency flux noise, motion in static Earth's field due

to vibration and displacement of mobile SCE instrumentation, etc., may result in parameter change, noise, or loss of flux lock in SQUID magnetometers. All these deleterious effects affect properties and behavior of devices, circuits, and systems and must be prevented or at least adequately minimized by shields and other measures such as on-chip local pinning of penetrating vortices by antidots, moats, and other suitable local discontinuities in the superconducting layers, for example. Obviously, SQUIDs and SQUID-based devices such as SFQ cells, gates, and qubits are particularly vulnerable and therefore require particularly effective on-chip vortex traps, magnetic and electromagnetic shielding enclosures, preferably superconducting, and very careful electromagnetic shielding, e.g., by very thin metallized Mylar foils and multilayers. Shielding of scientific experiments, e.g., nuclear magnetic resonance (NMR) or search for electric dipole moment (EDM) and biomagnetic diagnostic systems require magnetic shielded rooms (MSRs) with walls of several sheet layers of high-permeability soft alloy (e.g., Mu-metal) and aluminum, compensation of static and low-frequency fields by the, so-called, active shielding, etc. General principles of magnetic and electromagnetic shielding are treated by textbooks, see for example [11, 12], which include design and calculations of shielding enclosures and their effectiveness. Shielding of large superconducting systems is discussed, e.g., in [13], of qubits in [14], and shielding by superconductors in [15]. With the advent of HTS, tubular can ceramic superconductor shields, especially those fabricated of Bi-2223, became popular and are available commercially. In practice, effective electromagnetic shielding often involves also a considerable amount of art based on acquired experience. Shielding measures for specific applications are mentioned in the following sections.

2.4 Cryogenics

Cryogenics is an auxiliary part of any electronic system incorporating SCE. The usual cryogenic enclosures are commercial vacuum and superinsulation-insulated dewars, usually filled with a liquid cryogen, either liquid helium (LHe) or liquid nitrogen (LN_2), providing two standard operating temperature levels—4.2 K for LHe and 77 K for LN_2. Commercial mechanical cryocoolers of various types can also provide wide intermediate T ranges. In the range below 77 K, one-stage Stirling cryocoolers are the most typical unless minimum of noise is required. In the range around 4.2 K, multistage Gifford-McMahon and pulse-tube cryocoolers are used, the latter if minimum of noise is essential. Temperatures somewhat lower than those of the liquid boiling point at one atmosphere can be obtained by pumping, i.e., reducing the pressure over the liquid surface, a rather inconvenient laboratory method. Quantum computing (QC) processors and communication links require temperatures much lower than that of LHe, for QC in the 10–50-millikelvin range, assured by commercial dilution refrigerators.

In the past two decades, the use of cryogenic cryocoolers has been expanding for LTS and HTS due both to technology and reliability improvements and, for LTS, to steadily increasing prices of LHe and its paucity. Cryocooling is likely to become the dominant SCE cooling mode of the future, with a trend towards integration into the equipment's housing to promote its "invisibility" and miniaturization for electronic applications, including even cooling on the chip. Generally, small cryocoolers typical for most LTS SCE systems are much less efficient than large plants used for liquefaction of LHe and cooling of various large-scale systems, such as particle accelerators, for example. For small machines, order of 1% of Carnot efficiency is typical. Relatively recent surveys of cryocooler performance are [16–19], but an up-to-date survey of small cryocoolers specifically for SCE is sorely needed.

3 Antennae and Filters

3.1 Antennae

Wireless RF communication in the wide range from hertz to terahertz requires signal transmitter and receiver antennae usually shaped as three-dimensional structures. Especially since the advent of HTS, very low surface (loss) resistance of superconductors leading to improved antenna efficiency stimulated studies of electrically small passive antennae (ESA), and superdirective small arrays of these, essentially for superconducting receivers.[4] Such antennae are usually used in conjunction with lenses or reflectors. Geometrical, electrical, and thermal limitations imposed by the necessity to use HTS epitaxial films on relatively high electric permittivity crystal substrates, and the necessity of using a cryogenic vacuum radome with a window transparent to incoming radiation in the operational RF band, but highly reflective to thermal radiation, limited such studies mainly to efficiently matching a normal antenna to the remaining superconductor circuitry. Small planar HTS antennae have sometimes been used in laboratory demonstrations of radiation and particle detectors and HTS intrinsic JJ oscillators. Fundamentals of passive small antennae, also superconducting, are given in existing textbooks [20–22]. A particular example of passive small

[4] Small compared with the wavelengths received.

superconducting antenna for the low-frequency range is the pickup coil of a SQUID magnetometer. It is sensitive to the electromagnetic field and, for example, effectively detects weak far-field signals induced underground in deep layers of mineral ores by electrical pulses of an external transmitting antenna in the TEM geomagnetic exploration method (see Section 6.2). I am not aware of any existing microwave ESA application in operating civilian systems of any kind.

A rather new development are superconducting quantum arrays (SQAs) or superconducting interference filters (SQUIFs) [23], first demonstrated in the past decade as filters and amplifiers. With proper bias, their output signal is a steep linear function of the input signal applied simultaneously to the whole spectrum of random loop dimensions. This and other properties are succinctly described in Section 6.3. Kornev and collaborators were first to investigate their usefulness as signal amplifying broadband antennae [24]. A summary of their multiple publications is included in [25]. Others have shown the broadband detection of far-field FM radio stations by such arrays made of Nb [26]. Such SQAs should be operable in the bandwidth from Hz to several or even tens of GHz in conjunction with SC analog to digital converters (ADCs). The next decade may bring reports of successful implementation of SQA antennae, e.g., in operating microwave satellite signal receivers.

3.2 Filters

Historically, in late 1990s, multipole superconducting filters became the first commercial HTS SCE industrial product for US mobile (cellular) telephony stations, due to a particularly dense and complicated allocation of commercial carrier sub-band, and thus greater need for high-performance multipole bandpass and bandstop filters with very sharp skirts (narrow transition widths δf_s between bandstop and bandpass frequencies). However, and rather soon, the advent of newer generations of mobile telephony obviated the need for superconducting filters, and their lasting acceptance was not attained. Today, RF filters are mostly of interest for superconducting digital receivers and other HF analog/digital (mixed) circuitry.

A multipole filter order n consists of n serially coupled identical planar resonators. The filter's fractional bandwidth $w = \Delta f / f_{0,}$ with Δf being the bandpass width and f_0 the resonant frequency of coupled resonators. The filter performance increases with n and with the unloaded resonator Q_u attained, as shown in Fig. 4. The insertion loss of such coupled-resonator filters is given by

$$\mathrm{IL} \approx n/Q_u w \,(\mathrm{dB}) \tag{5}$$

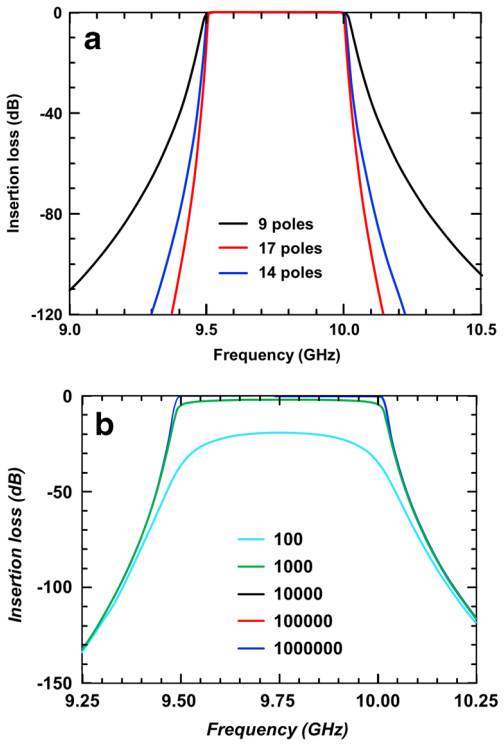

Fig. 4 **a** Example of microwave filter characteristics for three different pole numbers and very high unloaded Q_u. **b** Example of the 14-pole filter characteristics for different values of unloaded Q_u; approximately the same center frequency as in (**a**). Data courtesy of Oates [30]. With permission of CRC Press

Hence, a narrowband filter with set w, sufficiently high n, and low insertion loss must be build using very high Q_u resonators. Most of these filters are of Chebyshev or Cauer (elliptic) type and use either microstrip or lumped element technology.

The power handling capability of planar filters is limited to about 100 mW and sufficient for receiving devices, but not transmitters, where tens of watts are needed. Coupled dielectric disc 3D resonators can fulfill this requirement. Generally, at too high-power levels, nonlinear and other spurious effects appear and the filtering performance collapses.

Microstrip filters are discussed in [5, 27, 28], the superconducting lumped element ones in [29]. The most up-to-date review is [30], and this short section is in part based on it.

4 Amplifiers, Oscillators, and their Applications

4.1 Amplifiers

Foundations of SQUID RF amplifiers were laid by John Clarke and collaborators, at UC Berkeley and elsewhere,

between early 1980s and 2000s [31]. Devices studied were based on variants of the classical SQUID geometry design consisting of the bare DC SQUID loop in the form of a flux focusing square washer over which is deposited a thin insulating layer followed by a multiturn spiral input coil of inductance (L_i) tightly coupled to the SQUID loop inductance (L) by mutual inductance (M_i), see the schematic of Fig. 5. SQUID RF amplification, especially at microwave frequencies, is still in active development thanks to the interest in quantum circuits for computing and communication. The input/pickup circuit consists of the RF input signal source (V_i), pickup inductance (L_p), and capacitor (C_i) for resonant (tuned) operation in the fractional bandwidth $\delta f/f_0$, where f_0 is the resonance frequency and δf is given by bandwidth at half of the peak signal value. The SQUID is biased by bias current (I_b) and flux (Φ) to attain the optimum working point near maximum $\partial V/\partial \Phi$. At low frequencies, below about 1 MHz, only untuned amplifier (C_i eliminated or shorted) can provide an adequate bandwidth with gain (G) of about 20 dB or more. The gain of the tuned amplifier has a similar G level varying little up to about 100 MHz, where the G rolloff with increasing f begins due to the effect of parasitic capacitance between the L_i spiral and the washer (C_s). This capacitance can also cause spurious resonances that must be minimized by careful design. Various methods of reducing effects of C_s or exploiting these were demonstrated that permit to maintain a comparable level of G up to several gigahertz. Over the whole f range, the SQUID amplifier can have a very low noise temperature around T_N of 1 K at LHe temperature. Sufficiently below it, T_N can approach the quantum limit making it irreplaceable for scientific experiments and qubit readout vastly superior to HEMT amplifiers.

Comprehensive, but slightly dated reviews of the subject are given in [31, 32]. Of design approaches extending the operation to microwave frequencies, I like to mention the following:

(1) The microstrip SQUID where the input spiral coil has one free end. Thanks to C_s, the washer serves as the ground plane in which mirror image RF current is induced ([33] and refs. therein). At very low T, this type of SQUID is capable of approaching the quantum limit. This type is favored, e.g., in cosmology experiments, such as search for axion dark matter.

(2) An optimized variant of SQUID named superconducting low-inductance undulating galvanometer (SLUG) of extremely low L, that was first created by John Clarke in the mid-1960s and recently optimized for qubit readout [34–36]. At 6 to 7 GHz, it can provide $G \approx 20$ dB in a rather wide bandwidth, while providing reverse isolation superior to that of microwave isolators [37]. It is currently favored as a preamplifier for qubit readout. Its disadvantage is the thermal noise backaction, which can, however, be obviated by pulsed operation.

(3) The parametric amplifier (PA), and especially the Josephson PA (JPA), that can approach or attain the quantum limit, exhibit the lowest noise demonstrated thus far, and a reasonable gain, with G on the order of 10 dB, but suffers of a narrow bandwidth, limited dynamic range, and the need for a microwave pump source. The first can be overcome, e.g., by a JPA of single-ended design that includes an on-chip, high-bandwidth flux bias line [38] or by traveling wave geometry exploiting the nonlinear kinetic inductance of a superconducting transmission line [39]. However, the microwave pump source is unavoidable in any case, and this makes PA or JPA rather less attractive for quantum circuits than the SLUG, in spite of its somewhat higher noise. Nevertheless, JPA can be invaluable in scientific quantum experiments.

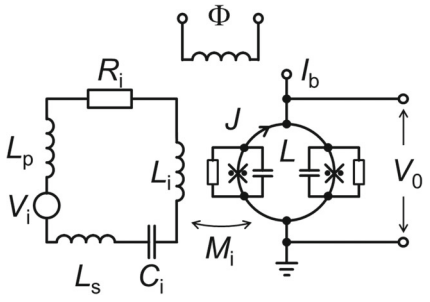

Fig. 5 Schematic circuit of a SQUID amplifier biased by current I_b and bias flux Φ. The input signal V_i is applied to the input circuit consisting of pickup coil L_p, matched to the input coil with inductance L_i tightly coupled to the SQUID via mutual input inductance (M_i). Also indicated is equivalent input resistance (R_i), the input capacitor (C_i), present only in the case of a tuned amplifier and the stray inductance L_s

4.2 Oscillators

There are no practical LTS oscillators exploiting the 2nd Josephson equation, mainly due to the difficulty in assuring needed output power of coherent radiation of large and highly uniform JJ arrays with a sufficiently narrow linewidth. The only type of superconducting oscillator currently operating in a realistic, in-field scientific application is that based on LTS long JJ flux-flow device (Section 2.2). Thanks to successful phase locking, this flux-flow oscillator (FFO) has linewidth between 1 and 5 MHz and output power sufficient to pump a matched SIS mixer. The FFO is incorporated as into an on-chip integrated, phase-locked superconducting heterodyne receiver

(SIR) [40, 41]. Such a device is periodically flying in a stratospheric balloon [42] of the mission terahertz and submillimeter limb sounder (TELIS). It is a three-channel superconducting heterodyne spectrometer for atmospheric research use of which one channel is using SIR. In its 2009 maiden flight over Sweden, that channel collected data proving the capability for high-resolution molecular spectroscopy of multiple gaseous species in the troposphere/stratosphere and is since used for collecting date in the 480- to 650-GHz frequency range [42]. One can expect insertion of SIR-type receivers in future such missions. Demonstrations of SIR usefulness included also analysis of exhaled air in medical surveys and measurement of terahertz radiation emitted from intrinsic JJ stacks [41].

In the c-direction of single crystals, the extreme anisotropy of HTS cuprates, such as bismuth–strontium–calcium cuprate (BSCCO, $Bi_2Sr_2CaCu_2O_{8+x}$), results in the formation of natural stacks of intrinsic JJs capable of emitting coherent radiation at terahertz frequencies from stacks containing several hundreds to thousands of JJs [43]. In the past decade, considerable effort was devoted to investigating properties of such stacks and possibilities of fabricating intrinsic oscillators for practical applications. The fabrication complexity is shifted in this case from junction fabrication to extraction of uniform BSCCO platelets from a bulk crystal, facilitated by ease of such crystal cleaving along the $a - b$ planes, and ingenuous carving out of a functional JJ stack [44, 45] ([46] and refs. therein). Work by several in-part collaborating groups indicated that coherence is promoted by cavity resonance of the stack. However, self-heating and fabrication constraints limit the height of a single mesa. Self-heating becomes more severe with the number of JJs and is aggravated by poor thermal conductivity along the c-axis of the BSCCO crystal. The understanding of various coherence promoting and emission-limiting mechanisms is still in progress. Best-attained coherent emission data are frequencies up to 2 THz, linewidths down to several megahertz, and emitted power of over 0.2 mW from a single mesa [47] and up to 0.6 mW from an array of three synchronized mesas [48]. By now, efforts in application as terahertz sources reached the stage of laboratory demonstrations, e.g., of terahertz imaging [49] or portable terahertz source ([50] and refs. therein). A relatively up-to-date review of HTS emitters exists [51].

5 Radiation and Particle Detectors for Astronomy and Optical Quantum Communication

5.1 Detector Types

Two decades ago, the main and important contribution of superconducting devices to astronomical activities was the use of niobium SIS tunnel junction heterodyne mixers for astronomy receivers in the radiation range of about 0.1 to 1 THz, in spite of their rather low saturation level [52, 53]. The importance of mixers did not diminish, but a paradigm change occurred thanks to the invention, development and deployment of novel bolometric radiation and particle sensors, able to cover a wide f range from sub-infrared up to X and γ-rays, namely voltage-biased transition edge sensors (TES) and microwave kinetic inductance detectors (MKIDs) [54, 55]. By now, they supplanted semiconductor detectors in large radio astronomy telescopes with multipixel cameras. This became possible due to the development and introduction of SQUID readout and multiplexing, which are dramatically reducing the heat load to cryocoolers. Currently, the largest such cameras, installed in dishes 10 m in diameter, have 1–2 $\times 10^4$ pixels, more with each new camera generation, with up to 10^6 in perspective. Another detector increasingly used in various scientific experiments is the metallic magnetic calorimeter (MMC) using a paramagnetic alloy, such as Au/Er and Ag/Er, as an energy absorber [56, 57]. All these detectors have excellent energy resolution, fast response time, and good linearity but are relatively slow. When incident energetic photons break Cooper pairs, the resulting quasiparticles (QPs) remain in thermodynamic equilibrium with excited phonons dissipating in the thin film substrate that acts as the thermal sink. A recent review of various bolometric (thermal) detectors for scientific cosmological searches can be found in [58].

At the same time, superconducting hot electron bolometers emerged that can be used both as bolometers and single photon detectors. At low temperatures, the latter (SNSPD[5]) feature both a very high quantum efficiency and extremely fast response, on the order of a few picoseconds in the case of LTS thin films [59]. These devices, arguably the most important new contribution to the SCE detector field, are suitable for very efficient detection of optical single photons with negligible dark counts. SNSPDs enabled the completely new field of long-distance optical quantum communication [60] while simultaneously extending frequency range of mixers up to 5 GHz. Such mixers were promptly tested and used in space [61]. Below, TES, MKID, and SNSPD devices are briefly highlighted.

TES Detectors Transition edge detector consists of a very small[6] and thin strip of low-T_c superconductor film, thermally only weekly connected to a thermal sink. It

[5] Acronym SNSPD most often stands for Superconducting Nanowire Single-photon Detector. However, more correctly, it should stand for Superconducting Nanostripe Single-Photon Detector, since the active element is a two-dimensional superconductor and not a one-dimensional nanowire.

[6] Just large enough to couple to the SQUID's pickup coil.

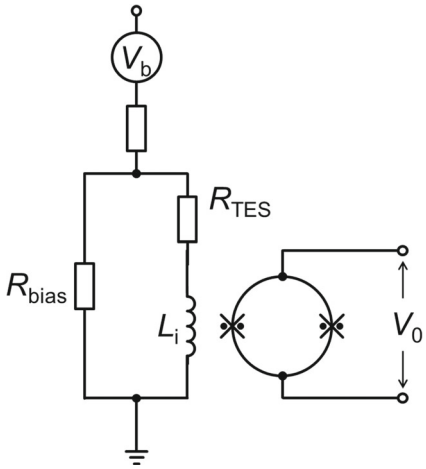

Fig. 6 Voltage-biased TES circuit with SQUID ammeter readout: the TES detector, represented by its resistance (R_{TES}), is connected in series with the SQUID input coil (L_i) and shunted by the bias resistor (R_{bias}) assuring constant voltage across $R_{TES} + L_i$. The bias source (V_b) is shown with its internal resistance; SQUID output is V_0

is voltage biased within the normal to superconducting state transition range and held at a very low temperature in the 10- to 100-mK range. Thanks to the very steep derivative, ∂V/∂T, of this transition, incidence of energetic photons or other particles breaking some Cooper pairs into quasiparticles, results in a large positive $\partial R_{TES}/\partial T$, i.e., a strong feedback between thermal and electrical power dissipated in the film. Voltage bias assures a negative electrothermal feedback and stabilizes the working point of the device [54]. Many materials are suitable for TES, either elemental metals (tungsten, W), low-T_c alloys (e.g., Al–Mn), or proximity bimetallic layers, e.g., of Mo–Au or Ti–Au. The current change resulting from temporary temperature raise is measured by SQUID. Schematic of the voltage-biased TES circuit is shown in Fig. 6. Current through the smaller shunting cold resistor (R_{bias}) assures voltage bias of the strip having resistance (R_{TES}) connected in a series with L_i of the SQUID ammeter. Its output signal voltage is multiplexed and magnified by a SQUID preamplifier. The review [62] provides details on TESs construction, properties, and applications.

Of the three worldwide largest cameras of the currently operating radio telescopes, two, namely the SCUBA-2[7] in Hawaii (wavelengths 0.45 and 0.85 mm) and the South Pole Telescope (SPT-SZ, SPT-3G, wavelengths 3.331, 1.99, and 1.362 mm), are equipped with TES pixel cameras. SCUBA utilizes time-domain multiplexing while SPT the frequency-domain alternative (see Section 5.2). Both have to their credit large numbers of new discoveries. SCUBA-2, operated by large international collaboration, has the all-sky astronomical survey as its main goal, while SPT already discovered hundreds of galaxy clusters and is concentrating on studies of cosmic microwave background (CMB) and determination of neutrino mass.

[7]Submillimeter common use bolometer array.

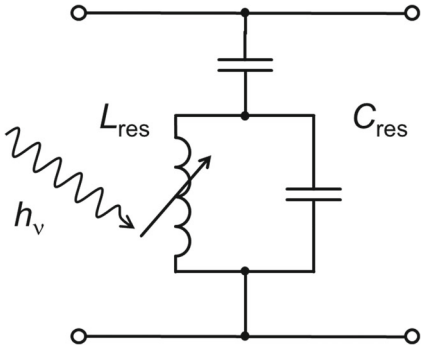

Fig. 7 MKID equivalent resonant circuit: energy of incident particle creates quasiparticles thus changing the kinetic inductance and detuning the resonator

MKID Detectors The third and youngest (2017) of the currently largest radio telescope with 10^4-pixel cameras, the DARKNESS,[8] is installed in the California's Mt. Palomar observatory, operates in the frequency range between 0.4 and 1.1 μm (infrared), and has as objective the discovery of dark exoplanets of relatively small stars. This camera, considered a pathfinder for future technologies of large cameras, utilizes MKID detectors.

The principle of superconducting kinetic detector is that the incidence of photons or other energetic particles generates quasiparticles of sufficiently low concentration that the sensing element remains in superconducting state (below T_c). Consequently, their effect is to change the kinetic inductance (L_{kin}) of a small thin-film segment inductively coupled to a very high-Q planar resonator circuit resonating at f_0 in the gigahertz range, see Fig. 7. Frequency shifts in this resonator's amplitude and phase, resulting from the temporary L_{kin} change, can be sensitively recorded when probed by a microwave signal. These changes are proportional to the incident energy. The detecting LTS element can be platinum silicide, for example. MKIDS were initially intended for sub-millimeter-range detection but are now increasingly used across the wide electromagnetic spectrum from infrared to X-rays. The review [63] covers MKID physics and applications.

5.2 Multiplexers

Of developed superconductor multiplexers, two types are used in large multipixel cameras: time- and frequency-domain circuits. In time-domain multiplexers, TES pixels

[8]Dark-speckle near-infrared energy-resolved superconducting spectrophotometer

are continuously biased, with readout SQUIDs of each column of an array connected in series and sequentially probed in time by switching bias from one SQUID to the next. In the frequency-domain approach, each pixel's resonator has a different f_0 and all pixels can be probed simultaneously by a comb generator signal. Signal from each pixel is then recovered by frequency-selective demodulators of room temperature electronics. An in-part comparative discussion of both approaches in application to TES arrays is given in chapter 8 of [31] while frequency-domain readout of large MKID arrays is discussed in [64].

5.3 Superconductor Nanostripe Single-Photon Detectors

The SNSPD detectors are based on a localized hotspot formation in a two-dimensional superconducting nanostripe [58, 65] and are directly related to hot electron bolometers (HEBs) pioneered by Gershenson et al. [66–68]. Their detection mechanism can be qualitatively described as follows [69]. An absorbed visible light quantum ($E \geq 2$ eV) excites an energetic QP of comparable energy which creates many secondary excited electrons, initially through electron-electron fast scattering and later, with falling energy, by electron-phonon (e-p) emission by QPs breaking even more Cooper pairs. This cascading QP multiplication continues until the secondary QPs approach the energy level of upper edge of the energy gap 2Δ of the superconductor. Very large internal gain, sufficient to attain single-photon energy resolution, results from this QP multiplication mechanism. The whole QP thermalization process takes about 7 ps for NbN, the generally used LTS nanostripe material [70], and less than 1 ps for YBCO [69]. Advantages of this type of detectors are many, including broadband performance and very low dark count. Hot electron bolometers can also be advantageously used as superior TES and MKID devices.

Niobium nitride is today the LTS material of choice for SNSPD devices, because it has the shortest e-p relaxation time constant and can be grown as ultrathin films of high quality suitable for nanopatterning of nanoscale single-photon devices, typically in the form of meander or spiral nanostripe structure. A schematic cross-section of such a planar device, about $10 \times 10 \mu$m in size, is shown in Fig. 8. In spite of its superior speed, YBCO is not used at present, because of overwhelming difficulty of nanoscale fabrication and on-chip integration processes.

The highlight above cannot do justice to the topic of HEB-based devices, but the references cited, especially the excellent most up-to-date reviews [65, 69] provide ample information.

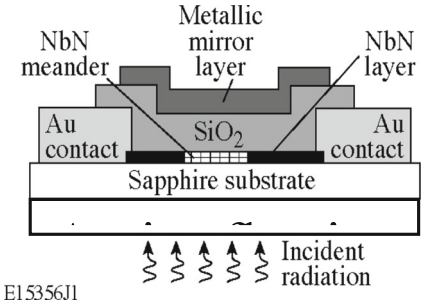

Fig. 8 Cross-section of SNSPD detector [69], with permission from the CRC Press

6 SQUID Magnetometers and other SQUID Applications

6.1 Signal Pickup and Readout

SQUIDs have multiple applications, of which some are mentioned in other sections. The earliest and quite important one is magnetometry. In contrast to SQUID amplifiers (Section 4.1), which have a narrow dynamic range sufficient for weak signals, magnetometers require excellent linearity over a very wide intensity range of measured magnetic field and flux. This is made possible through the use of flux-locked feedback loop which also provides extremely high resolution down to 10^{-6} to $10^{-7}\Phi_0$ for best LTS (niobium) SQUIDs. Figure 9 shows the generic block diagram of a flux modulation and feedback circuit. The typical dynamic range is > 120 dB. The slew rate at which the feedback can follow signal amplitude is in the range of 1–5 Φ_0/μs. More recently, to improve bandwidth, flux modulation is often replaced by direct readout with some form of positive feedback, which enhances SQUID's

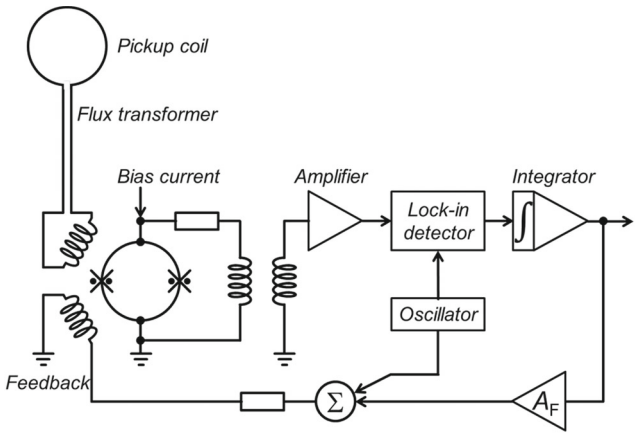

Fig. 9 Block diagram of frequency-modulation flux-locked readout circuit

sensitivity. Bandwidths in 10–20 MHz range are realistic. Double relaxation oscillation (DROS) readout has also been used in some cases. Usually, only the SQUID and step-up transformer within a superconducting shield are held at the cryogenic T, while the rest of the readout circuitry is at room temperature and included in the SQUID readout electronics, which also provides all biases and controls, nowadays computer controlled and automated. It has been for long time a commercial product in Europe, Japan, and the USA. A thorough review of all types of SQUID electronics with ample references is available in [71]. Latest improvements in magnetometer readout are presented in [72].

The typical magnetometer input circuit is the entirely superconducting flux transformer shown in Fig. 10. It consists of a pickup coil, either 3D or planar, which collects the signal to be measured and is linked via superconducting leads with the planar input coil of the SQUID, which today is always integrated on the chip as is the feedback coil. When measuring weak signals from localized sources in the presence of much stronger environmental fields, two coils can be connected in series opposite to exclude the common mode and obtain a 1st-order gradiometer in either 3D axial or planar configuration. The gradiometer order can be extended by adding more coils with correspondingly more turns. In attempts to construct very sensitive multichannel SQUID systems capable to operate without magnetic and electromagnetic shielding, even in the presence of many orders stronger external fields, commercial gradiometers of 2nd and 3rd order were demonstrated and manufactured but proved insufficient in arbitrary environments. In such uses, expensive and inconvenient MSRs are in most cases a necessity, e.g., in hospital environments in the case of noninvasive diagnostic systems measuring local fields of human brain (magnetoencephalography (MEG)), heart (magnetocardiography (MCG)), or spine (spinography). Extremely small pickup coils, also with flux-concentrating magnetic needle cores are used for various types of SQUID microscopes.

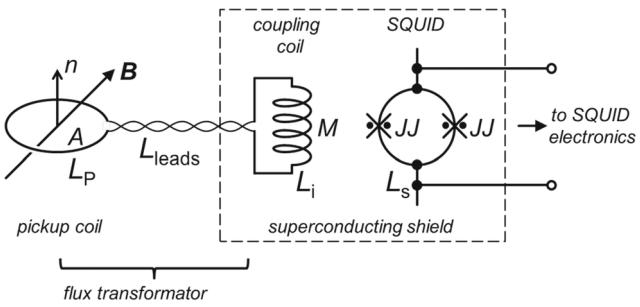

Fig. 10 Simplified schematic diagram of flux transformer inductively coupled to the SQUID. Parasitic inductances and capacitances are not shown. Only the pickup coil is outside of the superconducting shield. Everything shown is at the cryogenic temperature $T < T_c$, typically $T \approx 0.5\ T_c$ for Nb magnetometers and $T \approx 0.85\ T_c$ for HTS devices

6.2 Magnetometric Applications

Only a few examples of multiple magnetometric applications can be mentioned here. These and some other are properly covered in [4, 7, 8]. The first possible SQUID application was proposed in geomagnetism, already in 1960s, and was demonstrated by the team that discovered quantum interference and pioneered SQUIDs.[9] Also, the first truly successful industrial venture has been a small US company manufacturing rock magnetometers.[10] It is thus interesting that after three decades of investigating various geomagnetic prospecting methods, the first application with a very significant albeit indirect economic impact emerged in geomagnetic prospecting of mineral metallic ore deposits. It is the transient electromagnetics (TEM) method of contactless surveying, both ground-based and airborne [73, 74]. That success resulted mainly from pioneering efforts of Commonwealth Scientific and Industrial Research Organization (CSIRO) in Australia, and IPHT-Jena in Germany.[11] These teams developed portable HTS and LTS SQUID magnetometer systems capable of operating in motion in the presence of ambient static and electromagnetic fields orders of magnitude stronger than the measured signals, thanks also to judicious use of electromagnetic shielding. TEM is an active time-domain method in which strong pulse sequences from a transmitter result in very weak secondary electromagnetic field $B(t)$ response signals due to currents induced deep in the ground. Surveys hundreds of meters deeper into the ground than when using conventional room-temperature inductive coil TEM receivers that measure $\partial B/\partial t$ thus became possible. The use of SQUIDs permits to measure decaying signals N times longer which produces about $N^{1/2}$ times deeper recorded data. This difference proved decisive in discoveries of deeper mineral ore deposits on three continents (Africa, Australia, North America). Only in the first decade of SQUID use, the value of these deposits has been estimated at much more than US$50 billion. The number of SQUID surveying systems in use remains small. Another increasingly successful surveying method, the tensor magnetometry, is covered in the two references cited above.

In terms of industrial instrumentation products, SQUID susceptometers [75] permitting one to measure magnetic susceptibility of material samples became probably the biggest commercial SQUID magnetometry success to date.

[9] Ford Scientific Laboratories, Dearborn, MI, USA.

[10] 2G Enterprises, founded by the late Bill Goree in 1978.

[11] IPHT is the German acronym of the Institute for Photonics and Advanced Technology; IPHT is located in Jena, Germany.

The discovery of HTS cuprates and searches for other HTS materials prompted very large number of laboratories to acquire such instruments [76]. The LTS SQUID itself is just a small component enabling sales of a relatively large self-contained instrument including a superconducting magnet, sophisticated controls, and more recently also a compact mechanical cryocooler.

An application, into which enormous effort has been and is still being invested since the 1970s, is the biomagnetic research using diagnostic instrumentation [77, 78] and the related software, especially for approximate solutions to the inverse problem [79]. Several diagnostic methods have been developed and tested, also in realistic clinical environments. Of these, the magnetoencephalography, which images and interprets the local distribution of magnetic fields due to neuronal currents, is used in brain, psychology, and even language research. However, the total number of such systems installed worldwide is low, somewhere between one and two hundred. While clinical uses were convincingly demonstrated, e.g., in presurgical localization of epileptic foci, wide clinical acceptance is missing due to high cost including the necessary MSR and insufficiently attractive cost/benefit ratio. Even less accepted for the same reason is magnetocardiography, the imaging of local heart fields using similar systems, with only few hospitals worldwide successfully practicing it [80], in spite of numerous preliminary clinical studies showing clear patient benefits, e.g., in noninvasive screening of ischemia suspects or fetal (prenatal) diagnostics.

The last, but not least application of SQUID magnetometry that should be mentioned here is the nondestructive evaluation of materials and structures (NDE) using SQUID magnetometers or gradiometers [81, 82]. In many cases, it faces technical problems and uses solutions similar to those of geomagnetic SQUID applications, e.g., in requiring portability, operation while in motion, and immunity to much stronger environmental fields without using magnetic shielding of the superconducting pickup coil systems or antennae. It is important to note that SQUID NDE is usable also to test metallic materials and structures that are not magnetic. In this case, by inducing eddy currents with the help of a local transmitter, one measures local magnetic signatures of eddy current anomalies in tested objects.

The acceptance of SQUID NDE is currently limited to rare cases where the cost/benefit ratio is attractive enough, or where no other solution exists, as is the case in testing niobium sheets for very-high-Q cavities used in particle accelerators. In the recent past, SQUID NDE was in one case used in industry for testing airplane parts, e.g., turbine discs, where risk of ferromagnetic inclusions existed. In this case, the use of SQUIDs was eventually discontinued in favor of a fluxgate magnetometer, in spite of a major sensitivity reduction. In the 1990s, extremely successful

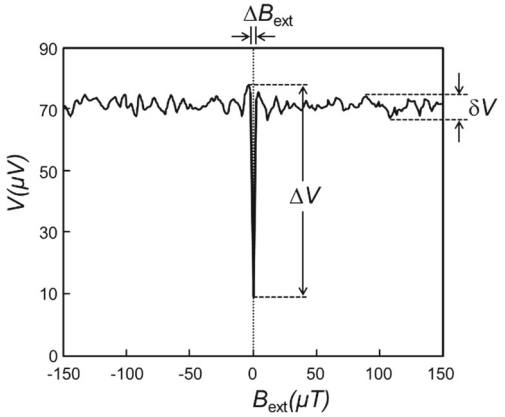

Fig. 11 SQUIF: typical experimental DC output voltage response to external field of an early parallel SQUIF with 30 JJs (courtesy of N. Schopol 2009, unpublished). The amplitude of the singularity is ΔV, the peak-to-peak noise amplitude δV

were in-field demonstrations of invisible cracks detection in metallic tendons of concrete highway bridges using portable HTS SQUIDs. Nevertheless, broader introduction of SQUIDs for periodic bridge testing did not follow due to economic/cost reasons. The hour of HTS SQUIDs in such applications may still come with ageing of most bridge structures in developed countries and major disasters such as the most recent catastrophic collapse of the Genoa freeway bridge (August 2018).

6.3 New Developments, other Applications

Of developments of the last two decades, I briefly highlight only two: nano-SQUIDs for metrology and microscopy and SQUIF arrays. Nano-SQUIDs are well covered by the review [83], and their metrological uses are discussed in [97]. SQUIFs, already mentioned in Section 3.1, have been theoretically analyzed [23] and experimentally investigated with great success under the leadership of Niels Schopol.[12] Actually, the idea came from an earlier theoretical work by Carelli et al., who first proposed a novel absolute SQUID magnetometer array with incommensurable loop areas but were not successful experimentally [84]. Schopol's group's experiments showed that in both parallel and serial arrays or a combination of both, certain quasi-random loop-size distributions, analogous to unconventional grating structures, result in coherent Josephson oscillations in the array with the DC voltage response exhibiting a singularity, i.e., a sharp global minimum at $B = 0$ with very steep transfer function $\partial V/\partial B$, as shown in the example of Fig. 11. The usefulness of SQUIFs as weak signal amplifiers and amplifying antennae was convincingly demonstrated.

[12] At the University of Tübingen, Germany.

Future in-field applications, e.g., as antennae in microwave receivers can be expected.

7 Metrology Instrumentation

Of all applications of SCE devices to metrology, Josephson voltage standards (JVS) are excellent examples of very important applications where capabilities of SCE are unique. Pioneering development of JVS started in the early 1970s at NIST-Boulder[13] [85] and continues until today thanks to ever new improvement concepts contributed by several National Metrology Institutes (NMI), especially the National Institute of Standards and Technology (NIST)-Boulder and PTB-Berlin[14] [86], partly in fruitful collaboration. JVS are also first examples of successful LSI of JJs. Of many reviews already published on the subject, the most up-to date is probably [87].

Conventional Josephson Voltage Standard The principle of the now-conventional JVS (CJVS) derives directly from the second Josephson equation linking the voltage and frequency only by the ratio of fundamental constants e and h defining the Josephson constant $K_J = 2e/h = 483\ 597.8525 \times 10^9$ Hz/V, the value agreed upon by all NMI. Its standard uncertainty is 0.003×10^9 Hz/V. As the frequency can be measured with very-high accuracy, it defines the accuracy of the volt. Irradiation of a large array of nearly identical JJs biased into voltage state with uniform microwave distribution results in Shapiro steps at voltages $V = n/K_J$, where n is the integer number of a step. In the I - V curve of a highly hysteretic JJ array driven by signal frequency of usually 70 GHz, multiple initial current steps conveniently cross the zero voltage line at precisely known sum voltages (Fig. 12). With a suitable termination load, crossing(s) of the load line with the zero-voltage step(s) define the working point(s).

After a nearly quarter century of development, the present 10 V standard system consists of a cryostat with large magnetically shielded microwave-fed series/parallel array of $NbAlO_x$ JJs embedded into microstrip lines with identical terminations and the room-temperature electronics with the attending microwave circuitry, frequency counter, computer selecting the working point, etc., see [85] for details. Currently, turnkey commercial systems manufactured in the USA and Germany include a mechanical cryocooler. Today, CJVS are made also in Japan and China.

Programmable Voltage Standard While CJVS are acceptable for DC voltage measurements, they have some stability problems (noise-caused jumps from one step to the adjacent one) and are not suitable for tasks of growing importance that require rapid selection of the working point, such as rapid analysis of analog-to-digital and digital-to analog converters (ADC and DAC) and synthesis of accurate AC waveforms. To address such new tasks, two new types of JVS have been conceived, developed, and demonstrated by NIST: the programmable JVS (PJVS) and the Josephson arbitrary waveform synthesizer (JAWS). Both were first demonstrated in the last decade of XX century.

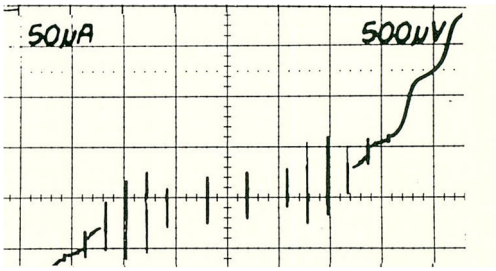

Fig. 12 Oscilloscope trace showing zero-crossing current steps on the I-V curve of an irradiated hysteretic JJ array (courtesy of C. Hamilton 2018, unpublished)

To make PJVS possible, the technology of internally shunted damped JJs having $\beta_c < 1$ had to be developed first to avoid parasitic inductances of external shunts. This was accomplished first with SNS junctions having rather low resistance Pd–Au barriers and practically zero capacitance. They necessitated using drive frequency of only 8 GHz. To make possible the usual drive of 70 GHz, tunable semiconductor Nb_xSi_{1-x} barriers were eventually introduced with Nb content near the metal-insulator transition [88]. Their resistance can be tuned by varying the niobium content x. Eventually, NIST and PTB demonstrated together first 10 V arrays driven by 70 GHz and containing near 70,000 JJs [89].

Figure 13 shows the simplified schematic design of a PJVS (a) and the $I - V$ curve of a single JJ (b). The output voltage $V = nf/K_J$ is defined by digitally programming the number of steps n. Each junction is biased only to $n = -1$, $n = 0$, and $n = +1$ steps, and large voltages are obtained by using very large arrays, as in CJVS. The result are large operating margins, i.e., the range of I over which every JJ is biased on the same constant V step. The circuit of PJVS is divided into binary sequence of array segments. Each segment can be set to $n = -1$, 0, or 1 steps by bias $-I_s$, 0, and $+I_s$. The combined step number N for the whole array can be set to any integer value between $-M$ and $+M$, where M is the total number of JJs. The circuit can also generate a staircase approximation to a sine wave by selecting steps in rapid succession [85] but is not the convenient and preferred solution in such applications.

Direct comparisons between CJVS and PJVS indicated agreement better than 1 part in 10^{10} ([90] and refs. therein).

[13] Formerly the National Bureau of Standards, NBS, USA.

[14] PTB is the German acronym of the Physikalisch-Technische Bundesanstalt, the German National Metrology Institute.

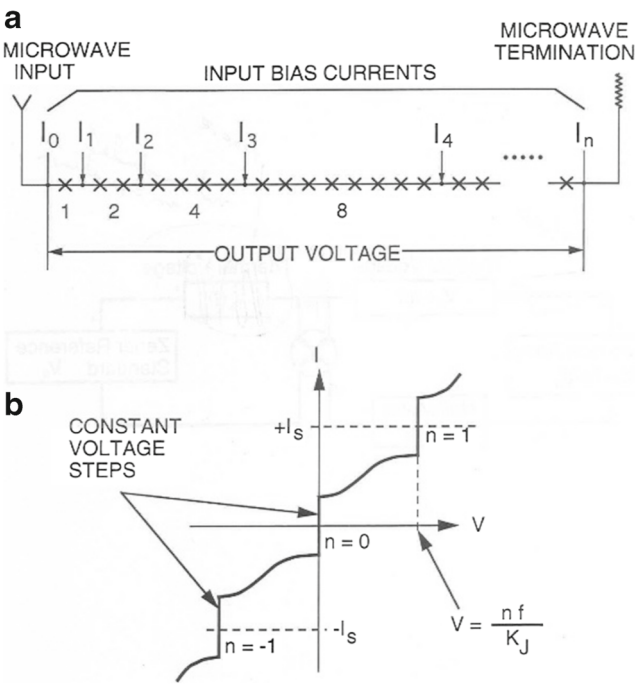

Fig. 13 **a** Simplified schematic design of PJVS, old JJ symbols are used. **b** Voltage steps $n = -1, 0$, and $+1$ of a damped JJ [85] (courtesy of Hamilton 2018)

Consequently, the replacement of CJVS by PJVS will have no effect on the accuracy of calibration.

Josephson Arbitrary Waveform Synthesizer Generation of arbitrary waveform with great accuracy became practical with the invention and demonstration of the Josephson Arbitrary Waveform synthesizer (JAWS) [91]. In JAWS, a series array of damped JJs is pulse driven by a variable frequency train of pulses. The principle block diagram and driving pulse train and the synthesized sine wave output are schematically shown in Fig. 14 [85]. In contrast to standards with sine wave drive, it features wide operating margins from 0 to about 30 GHz. The output voltage tracks the pulse repetition frequency so that the circuit is basically a digital-to-analog converter with fundamental accuracy. When synthesizing an arbitrary waveform, it eliminates transient errors that plagued CJVS and PJVS. In two decades of continuing development, the milestone of 1 V and the development paths towards higher voltage output have been demonstrated [92–94].

The PJVS and JAWS can be seen as complementary standards. Current direct DC comparison of the two standards indicated agreement to 1 part in 10^8 and permitted to identify sources of residual errors in JAWS [95], Further details and references to both standards can be found, e.g., in [87].

In 2019, the upcoming redefinition of the SI international system will make of JVS the direct realization of the unit

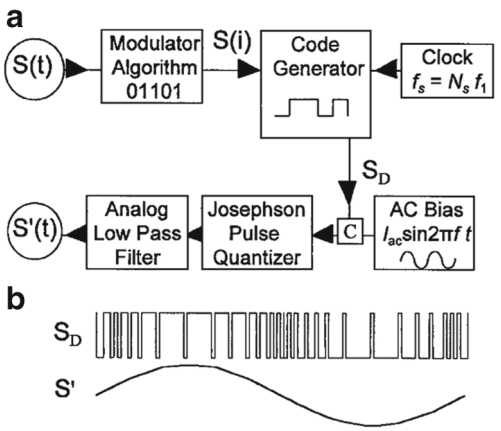

Fig. 14 **a** JAWS circuit block diagram. **b** The programmed pulse train of the code generator and the synthesized sine wave output [85] (courtesy of Hamilton 2018)

volt rather than a representation of the volt. After that, and with frequency standard traceable to SI units base, the unit volt will be independently realized in every calibration laboratory [90].

Metrological applications involve also SCE devices and circuits other than the JVS, especially SQUIDs in noise thermometry, superconducting comparators, etc. These other applications are discussed in [96, 97].

8 Digital Electronics

8.1 Historical Developments

Only one relatively up-to-date review of superconductor digital electronics exists, and the reader is directed to it [98]. Reviews published earlier are all dated, while what follows are only brief highlights.

The first concept to use superconductors as switches (cryotron gates) for computers and a demonstration of first integrated cryotron digital circuit date back to 1950s [99, 100] and precede even the birth of Josephson junctions. Voltage level gate circuitry, using JJs as much faster switches was inspired by cryotrons [101] and pursued in a major IBM project from 1967 until 1983.[15] This "latching logic" was then abandoned as not advantageous enough compared with very large-scale integrated circuit (VLSI) semiconductor electronics. In Japan, an analogous Japanese Ministry of International Trade and Industry (1949–2001) (MITI)-sponsored effort continued until 1990 and resulted

[15] Also, at two other US companies (Sperry and TRW), superconductor computer technology was pursued with different materials and JJ fabrication approaches.

in the demonstration of an operating microprocessor with over 2×10^4 JJs and a small 4 K random access memory [102].

Already in 1985, a totally different concept emerged, which became known as the rapid single flux quantum (RSFQ) logic [103, 104]. This concept is based on bit coding in the single magnetic flux quantum, which assures very low energy and fast switching between binary states ($\approx 10^{-19}$ J/bit, order of ps/bit). It could be used not only for computer logic but also for mixed signal devices such as analog-to-digital (ADCs), digital-to-analog, and time-to-digital converters (DACs, TDCs) of performance far superior to their semiconductor counterparts [105].

In RSFQ, the binary states are represented by the presence or absence of Φ_0 in the SQUID loop that serves as the elementary cell. When Φ_0 enters or leaves the loop, the junction phase undergoes a 2π rotation and a short SFQ voltage pulse appears. Its peak value is $2I_0R_s \approx 1$ mV (with Nb JJs) and duration $\tau \approx \Phi_0/2I_0R_s$. Such pulse applied to another cell can switch its state. This way, information passes from one cell to another. A single bit logic operation requires several flux transitions with the total energy dissipation of $\approx 10^{-18}$ J/bit. While this sounds impressive, it is not the whole truth. The dc power supply dissipation in the resistive current biasing network of each cell shown in Fig. 15a is over an order of magnitude higher [106]. The RSFQ main advantage driving its development has been the high speed (clock rate) at still low overall power consumption. Major disadvantage has been the large SQUID cell size severely limiting the integration level, especially of random-access memory (RAM) circuits for which no promising concepts existed until recently. Furthermore, the parallel bias lines carry high currents, on the order of ampere for 10^4 JJs, and associated magnetic fields have to be shielded off, which is difficult. Also, the clock network requires a significant overhead in JJs number. For mixed signal devices, such as converters, all this has been less critical. Here, area-inefficient serial memories can be used. With the still-practiced micrometer-linewidth, fabrication process integration of up to 2×10^4 JJs on chip is attainable and typical. Consequently, after developing a complete library of logic gates, the rather low level of RSFQ development effort (after year 2003) concentrated on promising communication applications. In the past decade, it resulted in the first successful quasi-commercial product: an x-band all-digital receiver for satellite communication [105].

8.2 Energy-Efficient Computing

In the current decade, the energy efficiency became a growing major concern for CMOS and future computer technologies beyond Moore's law [107]. Caused by the runaway increase of power consumption by large servers for cloud computing, "big data", etc., it is becoming a new metrics, equally and even more critical than further improvements in computing speed. Improvements in energy efficiency are addressed by a multitude of methods, both by hardware and software means. In the case of RSFQ logic, the elimination of static power consumption became the immediate goal [108]. Alternative approaches currently in development either modify the dc bias or replace it by ac bias. In terms of funding, pursuit of such approaches infused new life into the development of RSFQ and superconductor memory technology. The Cryogenic Computing Complexity (C3) US Intelligence Advanced Research Projects Activity (IARPA) program is currently the main driving force in this development work [109]. It includes also a technological component necessary for up to exa-scale computing capacities: higher integration densities require a nanotechnology-level fabrication process with correspondingly higher JJ critical currents.

The energy-efficient RFSQ (ERSFQ) is one of the dc power line approaches where resistors in the dc current

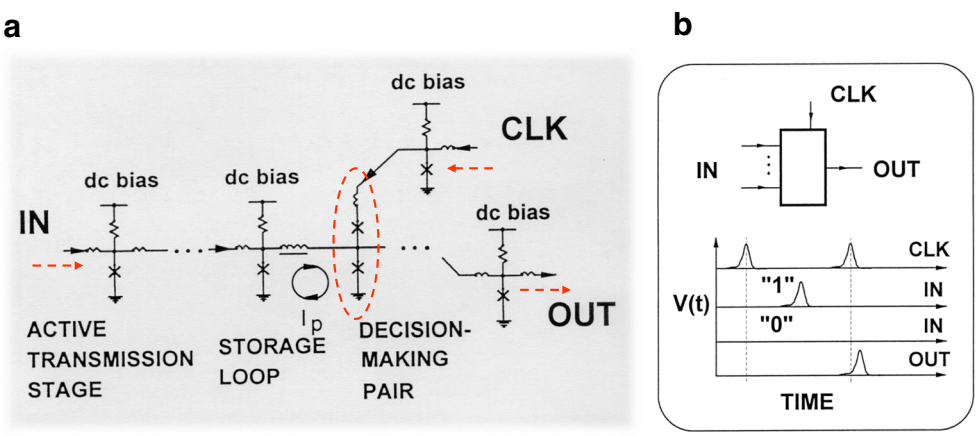

Fig. 15 **a** Schematic RSFQ circuit showing DC bias resistors, old JJ, and resistor symbols are used. CLK, abbreviation of the clock; I_p, pulse current [106]. **b** RSFQ pulse trains of the clock, binary "1," binary "0," and output from the decision pair, with permission from the CRC Press

biasing network are replaced by inductances and current-limiting JJs of an on-chip voltage biasing scheme [110]. This way the whole circuitry is superconducting while the library of already optimized RSFQ logic gates is still usable without modifications. However, this approach requires high inductance bias lines to maintain the operational margins and minimize the timing jitter. Small-scale large inductors may be obtained by introducing high-kinetic-inductance line layer. The clock speed of ERSFQ can still be maintained in the range of tens to possibly hundreds of GHz, as in RSFQ. Another version of resistor-free dc bias scheme is eRSFQ, which features synchronous phase balancing which eliminates phase unbalance and the timing jitter, but at the price of re-designing all logic gates.

The reciprocal quantum logic (RQL) is an AC biasing concept in which an AC transmission line is inductively powering the devices in series, with a four-phase AC clock providing directionality [111]. Here, "1" is encoded in a pair of pulses of opposite polarity, while the absence of such a pair encodes "0." The pulse pair resets the phase and thus avoids any phase unbalance. Another advantage is the relative simplicity of logic, which is combinational and low latency, like the CMOS semiconductor logic. Also, a low bit error rate was demonstrated for RQL. Compared with ERSFQ, the clock rate is expected to be lower, a possible disadvantage.

Dynamic power dissipation of 10^{-19} J/pulse is comparable in all non-adiabatic logic approaches, whether dc or ac powered. Orders of magnitude lower dynamic dissipation can be theoretically attained in adiabatic logic, of which most developed is that of the ac powered adiabatic quantum flux parametron (AQFP) based on an early concept of quantum flux parametron [112] but operated adiabatically. The energy change in adiabatic switching between energy potential wells was measured to be on the order of 10^{-20} J [113] with the possibility of further optimization by circuit design. The theoretical lower limit for irreversible switching is about 10^{-23} J [114]. Other advantages of AQFP compared with energy-efficient RFSQ concepts are easy routing without transmission lines and no-cost logic inversion. The disadvantage is the much lower operation frequency typical of the adiabatic processes and high latency. Improvement in both through multiexcitation AQFP [115], does not eliminate these drawbacks radically (Fourie, Univ. of Stellenbosch, private information). The AQFP approach is pursued in Japan.

Coming decade should show which of the current developmental approaches to energy-efficient superconductor logic and memory will be eventually adopted and whether any of them can offer sufficient advantages at least in some applications or not. Certainly, energy consumption per bit in SFQ and AQFP is lower by one to two orders of magnitude compared with all other prospective technologies beyond CMOS [107], and so is the extrapolated power consumption by future superconductor supercomputers (inclusive the cryocooling overhead) when compared with semiconductor computer technologies at the exascale performance level of 10^{18} floating point operations per second (flop/s) [108].

8.3 Random-Access Memory

Lack of scalable and real-estate-efficient concept of RAM plagued all pursued approaches to superconducting computing. In spite of major efforts, only a 4-kbit on-chip memory was attained in the MITI program [116], and after many years, a 64-kbit hybrid memory combining JJs with CMOS could be demonstrated [117]. Currently, pursued are various memory concepts and structures involving JJs with weakly and strongly ferromagnetic thin layers [118–122]. One example is the SIS'FS device structure, where S' is a very thin superconductor layer that may be affected by the ferromagnetic (F) layer [121]. Such junctions exhibit hysteretic behavior where magnetization switchable by magnetic field is switching the JJ critical current between two levels and can be made compatible with logic devices. A rather new result is the possibility of switching between 0 and π JJ behavior by spin-triplet supercurrent [123]. These various memory concepts offers the possibility of developing spintronic-like devices, such as the spin valve, for example, with promises of scalability, energy efficiency, and hopefully also acceptable real-estate demand. Some such concepts are developed in the C3 program, but none appears ripe enough to be highlighted here.

9 Qubits and Quantum Computing

Among the new applications of SCE, the superconductor quantum processors and prospective quantum computers are the most prominent novel application of Josephson junctions and SQUIDs. I offer only an arbitrary sampling of the subject and have to assume that the reader is familiar with principles of quantum mechanics and basic notions of quantum computing (QC), where N interacting (entangled) qubits can simultaneously represent 2^N values. Several reviews of qubit types and QC circuits using superconductivity exist [124–127].

Studies of macroscopic quantum coherence, see [9], and of the quantization of charge in the superconducting single-electron transistors (SETs), or, the so-called Cooper pair box ([128] and refs. therein), suggested that at sufficiently low temperatures, typically below 50 mK, JJs and SQUIDs can behave as artificial macroscopic atoms, i.e., are two-level systems that by applying pulse excitation of electromagnetic field could be brought into controlled quantum superposition of their two states and used as

an embodiment of qubits potentially suitable for quantum information processing by making such qubits quantum coupled and entangled. Indeed, in 1999 the first such device, a charge qubit, was demonstrated experimentally [129]. Two charge states, differing by $2e$ and coupled by tunneling of Cooper pairs,[16] were controllably brought into coherent superposition, although over a time of only $\tau \approx 1$ ns. In the following two decades, coherence times of various SQUID qubit types could be gradually extended by five orders of magnitude but remain still too short for effective quantum correction algorithms, thus resulting in low computing fidelity. Coherence below at least the millisecond range remains a significant disadvantage of SE compared with real atoms.[17] In the past 5 years, major causes of decay (decoherence) originating in qubit materials and electromagnetic environment were one-by-one identified and eliminated. To have magnetic field tunability, most qubit types are SQUIDs with the number of JJs between 1 and 3. Tunability, the relative ease in establishing controlled inter-qubit coupling and fabrication by a scalable and rather well-established thin film multilayer processing of integrated circuits are major advantages of SQUID-based qubits. Typical very low T_c superconductors for qubit and circuit fabrication are aluminum (Al) and titanium nitride (TiN).

It is not yet certain that SCE alone will be eventually the preferred QC technology rather than, for example, some combinations of SCE with semiconductor quantum dots and integrated optics. However, SCE is presently suitable for building functional small quantum processor hardware on a demonstrated and accessible to the public test user level of 20 interacting qubits [130] and between 49 and over 72 qubit level reportedly attained in 2017/2018 by the leading QC R&D industry teams, respectively, of IBM, Intel, and Google.[18] The latest claim is from Rigetti to having attained 128 qubits/chip. While the 20 qubit level is too low to demonstrate any advantage in calculation speed over classical quantum simulations (the "quantum supremacy"), it is believed that, for selected problems not requiring full-fledged quantum correction, a clear advantage can be demonstrated with an about 50 qubit processor [131]. At present, superconductor technology of qubits thus

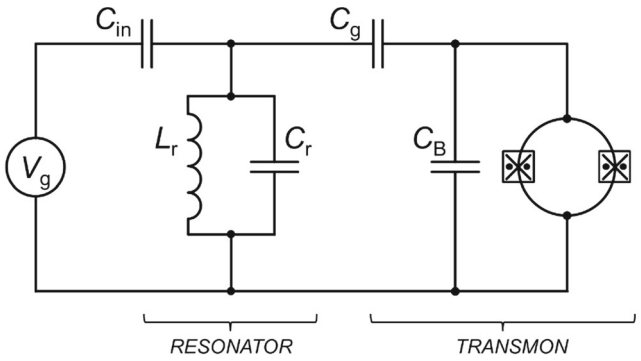

Fig. 16 Schematic diagram of the transmon. Josephson symbols in squares symbolize JJs of the Cooper box. The superconducting small island of that box between the SQUID and capacitor C_g is not shown

appears to be the preferred one, attracting the relatively largest institutional and industrial funding.

The discussion of various qubit types the reader may find in reviews listed above. Here, it suffices to say that today the advantageous and most generally used are various design variants of the transmon, a charge qubit, or Cooper pair box with the ratio of Josephson to charge energy $E_J/E_c >> 1$, coupled to a reasonably high-Q coplanar resonator, as shown in Fig. 16 [132, 133]. Fundamental mode of this resonator is far detuned from the qubit transition frequency which is also filtered to additionally suppress decay channels. This architecture makes possible coherent control, entanglement, and dispersive (resonator detuning) readout without additional circuitry. Preamplification of the readout and isolation from HEMT amplifier backaction is being done preferably by SLUG (see Section 4.1) operating near quantum limit. Among major advantages of all transmons is the much-reduced charge noise and the fact that the resonator can be used as a quantum bus permitting to entangle multiple qubits. An arbitrary example of a recent SQUID transmon designed for operating processors with larger number of qubits is described in [134]. Note, IBM is an exception among the leading teams and uses transmons with all-microwave, fixed-frequency two-qubit gates not involving SQUIDs but only JJs[19] [135].

An intriguing perspective for the more distant future of QC is topological QC with non-Abelian anyons, quasi-particle excitations that obey non-Abelian (commutative) statistics [136]. To that class of excitations belong the theoretically predicted localized Majorana[20] zero modes (MZM) in semiconductor nanowires that may be tuned to become topological superconductors when coupled to an s-wave superconductor [137–139]. Majorana fermions are

[16] Tunneling between their differing potential wells.

[17] Presently, 10 to 100 μs compared with minutes in the case of trapped ions. These are not readily scalable, but entanglement of several qubits was experimentally attained with trapped ions and simple quantum algorithms performed with high fidelity. In superconductor qubits, by one more order of magnitude, longer coherence time will be needed to implement quantum correction algorithms necessary for universal quantum computation.

[18] Thus far, there are no publications documenting this, only press releases.

[19] Advantages of the IBM transmon gates are insensitivity to flux noise and simpler control circuitry. Among disadvantages are the required very narrow tolerances on JJ I_0 and reduced speed of the gate.

[20] Majorana fermions are postulated quasiparticles that are their own antiparticles.

postulated quasiparticles that are their own antiparticles. Degenerate states associated with their zero modes should result in a topologically protected quantum memory and long-lasting coherence leading to an ideal embodiment for fault-tolerant quantum computation. Thus far, only indirect signatures of such degenerate states have been found experimentally through measurements of quantized conductance in InSb [140], or Shapiro steps in heterostructures of HgTe and Bi-doped Sb_2Te_3 with Al and Nb superconductors [141, 142]. Nevertheless, awaiting harnessing of MZM, scalable designs for topological QC have already been proposed [143]. Topological computation studies currently enjoy industrial support, mainly from Microsoft.

In closing, I should mention that very high numbers of superconducting circuits are also used in commercial d-wave quantum annealers, computing machines that may offer quantum speedup in solving certain classes of problems such as optimization, see for example [144, 145]. To date, there is no unambiguous and generally accepted confirmation of computing advantages claimed by the manufacturer [146]. Nevertheless, a few such relatively large machines incorporating 10^5 JJs have been sold and studies of quantum annealing continue at academia, research organizations, and industry. There is also an IARPA-sponsored effort to develop quantum enhanced computers.[21]

10 Concluding Summary and Outlook

As of today, SE is applied predominantly and very successfully in science, e.g., radio astronomy and cosmology, also in metrology, while gaining ground in exploration of minerals. Military, space, and quantum communication uses are slowly emerging and have assured bright future. Considerable efforts in developing industrial and medical applications, coinciding with the first 10–15 years after the discovery of HTS, resulted in many quite successful demonstrations of various industrial and clinical test instruments and large diagnostic systems. However, most has not been sufficiently advantageous and economically competitive to pass the test of time when used in realistic environments. Eventually, they did not gain widespread acceptance, although some still have some chances.

Until now, SCE has not matched the immense commercial success of MRI systems with superconducting magnets. Time will tell if the current efforts to save power in high-end computers will succeed with low-energy SCE digital logic gates. In the race to build quantum computers, SCE is the only technology that can produce both qubits and the high-speed low-power digital and mixed signal circuits that can control the qubits. This combination could prove decisive. Considering the high level of funding and effort, the outcome of this race, and of efforts towards high-end superconducting computers, is likely to be known in the next decade.

Acknowledgments I am indebted to the following colleagues for critically reading and commenting on the whole or part of the manuscript: David DiVinzenzo, John X. Przybysz, Roman Sobolewski, Elie K. Track, and Huabing Wang. Some of the references were kindly provided by Sam P. Benz, David DiVinzenzo, Valery Koshelets, John X. Przybysz, Allard Schnabel, Thomas Schurig, Marcel ter Brake, and Huabing Wang. Most of the figures were computer drawn by Dieter Lomparski. I owe sincere thanks to all those listed above.

References

1. Van Duzer, T., Turner, C.W.: Principles of Superconductive Devices and Circuits, 2nd edn. Prentice Hall. ISBN-13: 978-0132627429, ISBN-10: 0132627426 (1999)
2. Likharev, K.K.: Dynamics of Josephson Junctions and Circuits Gordon & Breach, Taylor & Francis, Ltd. (1992, 1996). ISBN: 3-88124-042-9 (1986)
3. Braginski, A.I.: Superconducting electronics: A dream or reality. Bull. Polish Acad. Sci. **48**(1), 57 (1997)
4. Seidel, P. (ed.): Applied Superconductivity: Handbook on Devices and Applications, vol. 2. Wiley (2015). ISBN-13: 978-3-27-741209-9, ISBN-10: 3527412093
5. Pozar, D.M.: Microwave Engineering, 4th edn. Wiley (2011)
6. Barone, A. (ed.): Principles and Applications of Superconducting Quantum Interference Devices. World Scientific Pub Co Inc, Singapore (1992). ISBN-13: 978-9810209117, ISBN-10: 9810209118
7. Clarke, J., Braginski, A.I. (eds.): The SQUID Handbook, vol. 1. Wiley (2004). ISBN: 3-527-40229-2
8. Clarke, J., Braginski, A.I. (eds.): The SQUID Handbook, vol. 2. Wiley (2006). ISBN-13: 978-3-527-40408-7, ISBN-10: 3-527-40408-2
9. Clarke, J., Cleland, A.N., Devoret, M.H., et al.: Quantum mechanics of a macroscopic variable: the phase difference of a Josephson junction. Science **239**, 992 (1988)
10. Braginski, A.I., Zhang Y.: Practical RF SQUIDs: Configuration and performance. In: Clarke, J., Braginski, A.I. (eds.) The SQUID Handbook, vol. 1. Wiley (2004). ISBN 3-527-40229-2
11. Rikitake, T.: Magnetic and Electromagnetic Shielding. Springer Science & Business Media, Kluwer (1987). ISBN-13: 978-9027724069, ISBN-10: 9027724067
12. Celozzi, S., Araneo, R., Lovat, G.: Electromagnetic Shielding. IEEE Press and Wiley Interscience (Wiley). ISBN: 978-0-470-05536-6 (2008)
13. Stuiber, S.A.: Creation of ultra-low remnant fields and homogeneous NMR fields for precision experiments. Ph. D. dissertation, Techn. Univ. München (2018)

[21] ODNI News Release No. 5-17, 24 April 2017, IARPA launches "QEO" program to develop quantum enhanced computers.

14. Kreikebaum, J.M., Dove, A., Livingston, W., et al.: Optimization of infrared and magnetic shielding of superconducting TiN and Al coplanar microwave resonators. Supercond. Sci. Technol. **29**, 104002 (2016)
15. Hamilton, W.O.: Superconducting shielding. Rev. Phys. Appl. **5**, 41 (1970)
16. ter Brake, H.J.M., Wiegerinck, G.F.M.: Low-power cryocooler survey. Cryogenics **42**, 705–718 (2002)
17. Kittel, P.: Cryocooler performance estimator. In: Miller, S.D., Ross, R.G. Jr.. (eds.) Cryocoolers 14. International Cryocooler Conference, Inc (2007)
18. Radebaugh, R.: Cryocoolers: The state of the art and recent developments. J. Phys.: Condens. Matter **21**, 164219 (2009)
19. Ladner, D.R.: Performance and mass vs. operating temperature for pulse tube and Stirling cryocoolers. In: Miller, S.D., Ross, R.G. Jr. (eds.) Cryocoolers 16. International Cryocooler Conference, Inc (2011)
20. Chaloupka, H.: Antennae. In: Cardwell, D., Ginley, D. (eds.) Handbook of Superconducting Materials. CRC Press (2003). ISBN-13: 978-0750308984, ISBN-10: 0750308982
21. Hansen, R.C.: Electrically Small, Superdirective, and Superconducting Antennas. Wiley. ISBN-13: 978-0471782551 (2006)
22. Hansen, R.C., Collin, R.E.: Small Antenna Handbook. Wiley. ISBN: 0470890835 (2011)
23. Häussler, C., Oppenländer, J., Schopol, N.: Nonperiodic flux to voltage conversion of series arrays of dc superconducting quantum interference devices. J. Appl. Phys. **93**, 1875–1879 (2001)
24. Kornev, V.K., Soloviev, I.I., Klenov, N., Mukhanov, O.A.: Design and experimental evaluation of SQUIF arrays with linear voltage response. IEEE Trans. A.pl. Supercond. **21**(3), 394–398 (2011)
25. Chaloupka, H.J., Kornev, V.K.: Antennae. In: Cardwell, D., Larbalestier, D. (eds.) Handbook of Superconducting Materials. CRC Press (2019). ISBN-13: 978-1439817308, ISBN-10: 1439817308
26. De Andrade, M.C., Leese de Escobar, A., Taylor, B.J., et al.: Detection of far-field radio-frequency signals by niobium superconducting quantum interference arrays. IEEE Trans. Appl. Supercond. **25**(5), 1603005 (2015)
27. Hong, J.-S., Lancaster, M.J.: Microstrip Filters for RF/Microwave Applications. Wiley (2001)
28. Shen, Z.-Y.: Microwave resonators and filters. In: Cardwell, D., Ginley, D. (eds.) Handbook of Superconducting Materials. CRC Press (2003). ISBN-13: 978-0750308984, ISBN-10: 0750308982
29. Chaloupka, H., Kolesow, S.: Design of lumped-element 2D RF devices. In: Weinstock, H., Nisenoff, M. (eds.) Microwave Superconductivity. Kluwer, Acad. Publ. (2001). ISBN-13: 978-1402004469, ISBN-10: 140200446
30. Oates, D.E.: Microwave resonators and filters. In: Cardwell, D., Larbalestier, D. (eds.) Handbook of Superconducting Materials. CRC Press (2019). ISBN-13: 978-1439817308, ISBN-10: 1439817308
31. Clarke, J., Lee, A.T., Mück, M., Richards, P.L.: SQUID voltmeters and amplifiers. In: Clarke, J., Braginski, A.I. (eds.) The SQUID Handbook, vol. 2. Wiley (2006). ISBN-13: 978-3-527-40408-7; ISBN-10: 3-527-40408-2
32. Mück, M., McDermott, R.: Radio-frequency amplifiers based on dc SQUIDs. Supercond. Sci. Technol. **23**, 093001 (2010)
33. Mück, M., Schmidt, B., Clarke, J.: Microstrip superconducting quantum interference device amplifier: Operation in higher-order modes. Appl. Phys. Lett. **111**, 042604 (2017)
34. Ribeill, G.J., Hover, D., Chen, Y.-F., et al.: Superconducting low-inductance undulatory galvanometer microwave amplifier: Theory. Appl. Phys. Lett. **110**, 103901 (2011)
35. Hover, D., Chen, Y.-F., Ribeill, G.J., et al.: Superconducting low-inductance undulatory galvanometer microwave amplifier. Appl. Phys. Lett **100**, 063503 (2012)
36. Hover, D., Zhu, S., Thorbeck, T., et al.: High fidelity qubit readout with the superconducting low-inductance undulatory galvanometer microwave amplifier. Appl. Phys. Lett. **104**, 152601 (2014)
37. Thorbeck, T., Zhu, S., Leonard, E.R. Jr.., et al.: Reverse isolation and backaction of the SLUG microwave amplifier. Phys. Rev. Applied **8**, 054007 (2017)
38. Mutus, J.Y., White, T.C., Jeffrey, E.: Design and characterization of a lumped element single-ended superconducting microwave parametric amplifier with on-chip flux bias line. Appl. Phys. Lett. **103**, 122602 (2013)
39. Eom, B.H., Day, P.K., LeDuc, H.G., Zmuidzinas, J.: A wideband, low-noise superconducting amplifier with high dynamic range. Nat. Phys. **8**, 623–627 (2012)
40. Koshelets, V.P., Shitov, S.V.: Integrated superconducting receivers. Supercond. Sci. Technol. **13**, R53–R69 (2000)
41. Dmitriev, P.N., Filippenko, L.V., Koshelets, V.P.: Applications in superconducting SIS mixers and oscillators: Toward integrated receivers. In: Wolf, E., Arnold, G., Gurvitch, M., Zasadzinski, J. (eds.) Josephson Junctions. History, Devices, and Applications, pp. 185–244. Pan Stanford Publ. (2017). ISBN-13: 978-981-4745-47-5, ISBN-10: 978-1-315-36452-0
42. de Lange, G., Birk, M., Boersma, D., et al.: Development and characterization of the superconducting integrated receiver channel of the TELIS atmospheric sounder. Supercond. Sci. Technol. **23**, 045016 (2010)
43. Tachiki, M., Iizuka, M., Minami, K., et al.: Emission of continuous terahertz waves with tunable frequency by intrinsic Josephson junctions. Phys. Rev. B **71**, 71(134515) (2005)
44. Ishida, H., Okanoue, K., Hamasaki, H., et al.: Self-planarizing process for the fabrication of $Bi_2Sr_2CaCu_2O_x$ stacks. Appl. Phys. Lett. **122503**, 86 (2005)
45. Wang, H.B., Wu, P.H., Yamashita, T.: Stacks of intrinsic Josephson junctions singled out from inside $Bi_2Sr_2CaCu_2O_{8+x}$ single crystals. Appl. Phys. Lett. **7**, 4010–4012 (2001)
46. Yurgens, A.A.: Intrinsic Josephson junctions: Recent developments. Supercond. Sci. Technol. **13**, R85–R100 (2000)
47. Sun, H., Wieland, R., Xu, Z., et al.: A compact high-T_c superconducting terahertz emitter operating up to 86 Kelvin. Phys. Rev. Appl. **10**, 024041 (2018)
48. Benseman, T.M., Gray, K.E., Koshelev, A.E., et al.: Powerful terahertz emission from $Bi_2Sr_2CaCu_2O_{8+\delta}$ mesa arrays. Appl. Phys. Lett. **103**, 022602 (2013)
49. Tsujimoto, M., Minami, H., Delfanazari, K., et al.: Compact superconducting terahertz source operating in liquid nitrogen. Phys. Rev. Applied **3**, 024006 (2015)
50. Hao, L.Y., Yuan, M., Ji, J., An, D.Y., et al.: Compact superconducting terahertz source operating in liquid nitrogen. Phys. Rev. Appl. **3**, 024006 (2015)
51. Welp, U., Kadowaki, K., Kleiner, R.: Nat. Photonics **7**, 702–710 (2013)
52. Blundell, R., Winkler, D.: The superconductor-insulator-superconductor mixer receiver—a review. In: Costabile, G., Pagano, S., Pedersen, N.F., Russo, M. (eds.) Nonlinear Superconductive Electronics and Josephson Devices, pp. 55–72. Plenum Press, New York (1991). ISNB: 13: 978-14613-6719-2, ISBN-10: ISBN-13: 978-14615-3852-3
53. Winkler, D.: Superconducting mixers. In: Cardwell, D., Ginley, D. (eds.) Handbook of Superconducting Materials. CRC Press (2003). ISBN-13: 978-0750308984, ISBN-10: 0750308982
54. Irwin, K.D.: An application of electrothermal feedback for high-resolution cryogenic particle detection. Appl. Phys. Lett. **66**, 1998–2000 (1995)

55. Day, P.K., Leduc, H.G., Benjamin A Mazin, B.A., et al.: A broadband superconducting detector suitable for use in large arrays. Nature **425**(6), 817–821 (2003)
56. Fleischmann, A., Enss, C., Seidel, G.: Metallic magnetic calorimeters. In: Enss, C. (ed.) Cryogenic Particle Detection. Topics Appl. Phys., vol. 99, pp. 149–201. Springer (2005)
57. Kim, I., Jo, H.S., Kang, C.S., et al.: Application of metallic magnetic calorimeter in rare event search. Supercond. Sci. Technol. **30**, 094005 (2017)
58. Pirro, S., Mauskopf, P.: Advances in bolometer technology for fundamental physics. Annu. Rev. Nucl. Part. Sci. **67**, 161–181 (2017)
59. Gol'tsman, G., Okunev, O., Chulkova, G., et al.: Picosecond superconducting single photon optical detector. Appl. Phys. Lett. **79**, 705–707 (2001)
60. Miki, S., Fujiwara, M., Jin, R.B.: Quantum information networks with superconducting nanowire single-photon detectors. In: Hadfield, R.H., Johansson, G. (eds.) Superconducting Device in Quantum Optics. Springer Intl. Publ. (2016). ISBN-13: 97-3-319-24089-3, ISBN-10: 978-3-319-24091-6
61. Cherednichenko, S.V., Drakinskiy, V.T., Berg, P., et al.: Hot-electron bolometer terahertz mixers for the Herschel space observatory. Rev. Sci. Instrum. **79**, 034501 (2008)
62. Ullom, J.N., Bennett, D.A.: Review of superconducting transition-edge sensors for X-ray and gamma-ray spectroscopy. Supercond. Sci. Technol. **28**, 084003 (2015)
63. Zmuidzinas, J.: Superconducting microresonators: physics and applications. Ann. Rev. Cond. Matter Phys. **3**, 169 (2012)
64. McHugh, S., Mazin, B.A., Serfass, B., et al.: A readout for large arrays of microwave kinetic inductance detectors. Rev. Sci. Instrum. **83**(4), 4702 (2012)
65. Korneev, A., Semenov, A., Vodolazov, G.N., et al.: Physics and operation of superconducting single-photon detectors. In: Wördenweber, R., Vanacken, J. (eds.) Superconductors at the Nanoscale: from Basic Research to Applications, pp. 279–308. De Gruyter Press (2017)
66. Gershenson, E.M., Gershenson, M.E., Gol'tsman, G.N., et al.: Heating of quasiparticles in a superconducting film in the resistive state. Pis'ma Zh Eksp. Teor. Fiz. **34**(5), 281–285 (1981)
67. Gershenson, E.M., Gershenson, M.E., Gol'tsman, G.N., et al.: Electron-phonon interaction in ultrathin Nb films. Zh. Eksp. Teor. Fiz. **97**(3), 901–911 (1990)
68. Semenov, A.S., Gol'tsman, G.N., Sobolewski, R.: Hot-electron effect in superconductors and its applications for radiation sensors. Supercond. Sci. Technol. **15**, R1–R16 (2002)
69. Sobolewski, R.: Optical sensors. In: Cardwell, D., Larbalestier, D. (eds.) Handbook of Superconducting Materials. CRC Press (2019). ISBN-13: 978-1439817308, ISBN-10: 1439817308
70. Il'in, K.S., Lindgren, M., Currie, M., et al.: Picosecond hot-electron energy relaxation in NbN superconducting photodetectors. Appl. Phys. Lett. **76**, 2752 (2000)
71. Drung, D., Mück, M.: SQUID electronics. In: Clarke, J., Braginski, A.I. (eds.) The SQUID, vol. 1. Wiley (2004). ISBN: 3-527-40229-2
72. Zhang, Y., Dong, H., Krause, H.J., Xie, X.: SQUID Readout Electronics and Magnetometric Systems for Practical Applications. Wiley. ISBN-13: 978-3-527-34488-8 (2020)
73. Clem, T., Foley, C.P., Keene, M.N.: SQUIDs for geophysical survey and magnetic anomaly detection. In: Clarke, J., Braginski, A.I. (eds.) The SQUID Handbook, vol. 2. Wiley (2006). ISBN-13: 978-3-527-40408-7; ISBN-10: 3-527-40408-2
74. Stolz, R.: Geophysical exploration. In: Seidel, P. (ed.) Applied Superconductivity: Handbook on Devices and Applications, vol. 2. Wiley (2015). ISBN-13: 978-3-27-741209-9, ISBN-10: 3527412093
75. Blake, R., Wellstood, F.: Measurements of magnetism and magnetic properties of matter. In: Clarke, J., Braginski, A.I. (eds.) The SQUID Handbook, vol. 2. Wiley (2006). ISBN-13: 978-3-527-40408-7; ISBN-10: 3-527-40408-2
76. Sager, R.: SQUIDs-from laboratory devices to commercial products. In: Rogalla, H., Kes, P. (eds.) 100 Years of Superconductivity. Taylor & Francis Ltd (2011). ISBN-13: 978-1-4398-4946-0
77. Vrba, J., Nenonen, J., Trahms, L.: Biomagnetism. In: Clarke, J., Braginski, A.I. (eds.) The SQUID Handbook, vol. 2. Wiley (2006). ISBN-13: 978-3-527-40408-7; ISBN-10: 3-527-40408-2
78. Nowak, H.: SQUIDs in biomagnetism. In: Seidel, P. (ed.) Applied Superconductivity: Handbook on Devices and Applications, vol. 2. Wiley (2015). ISBN-13: 978-3-27-741209-9, ISBN-10: 3527412093
79. Lima, E.A., Irimia, A., Wikswo, J.P.: The magnetic inverse problem. In: Clarke, J., Braginski, A.I. (eds.) The SQUID Handbook, vol. 2. Wiley (2006). ISBN-13: 978-3-527-40408-7; ISBN-10: 3-527-40408-2
80. Inaba, T., Nakazawa, Y., Yoshida, K., et al.: Routine clinical heart examinations using SQUID magnetocardiography at University of Tsukuba Hospital. Supercond. Sci. Technol. **30**, 114003 (2017)
81. Krause, H.-J., Donaldson, G.: Nondestructive evaluation of materials and structures using SQUID. In: Clarke, J., Braginski, A.I. (eds.) The SQUID Handbook, vol. 2. Wiley (2006). ISBN-13: 978-3-527-40408-7; ISBN-10: 3-527-40408-2
82. Krause, H.-J., Mück, M., Tanaka, S.: SQUIDs in nondestructive evaluation. In: Seidel, P. (ed.) Applied Superconductivity: Handbook on Devices and Applications, vol. 2. Wiley (2015). ISBN-13: 978-3-27-741209-9, ISBN-10: 3527412093
83. Granata, C., Vettoliere, A.: Nano superconducting Interference device: a powerful tool for nanoscale investigations. Phys. Rep. **614**, 1–69 (2016)
84. Carelli, P., Castellano, M.G., Flacco, K., et al.: An absolute magnetometer based on dc superconducting interference devices. Europhys. Lett. **39**, 569–574 (1997)
85. Hamilton, C.A.: Josephson voltage standards. Rev. Sci. Instr. **71**(10), 3611–3623 (2000)
86. Niemeyer, J.: How the DC array standards were developed. In: Rogalla, H., Kes, P. (eds.) 100 Years of Superconductivity. Taylor & Francis Ltd (2011). ISBN-13: 978-1-4398-4946-0
87. Kohlmann, J.: Application to Josephson voltage standards. In: Wolf, E., Arnold, G., Gurvitch, M., Zasadzinski, J. (eds.) Josephson Junctions. History, Devices, and Applications, pp. 359–383. Pan Stanford Publ. (2017). ISBN-13: 978-981-4745-47-5, ISBN-10: 978-1-315-36452-0
88. Baek, B., Dresselhaus, P.D., Benz, S.P.: Co-sputtered amorphous Nb_xSi_{1-x} barriers for Josephson junction circuits. IEEE Trans. Appl. Supercond. **16**, 1966–1970 (2006)
89. Müller, F., Behr, R., Weimann, T., et al.: 1 V and 10 V SNS programmable voltage standards for 70 GHz. IEEE Trans. Appl. Supercond **19**, 981–986 (2009)
90. Rüfenacht, A., Flowers-Jacobs, N., Benz, S.: Impact of the new generation of Josephson voltage standards in ac and dc electric metrology. Metrologia **56**(5), S152–S173 (2018)
91. Benz, S.P., Hamilton, C.A.: A pulse driven programmable voltage standard. Appl. Phys. Lett. **68**, 3171–3173 (1996)
92. Flowers-Jacobs, N.E., Waltman, S.B., Fox, A.E., et al.: Josephson arbitrary waveform synthesizer with two layers of Wilkinson dividers and a FIR filter. IEEE Trans. Appl. Supercond. **26**(6), 1400307 (2016)
93. Brevik, J.A., Flowers-Jacobs, N.E., Fox, A.E., et al.: Josephson arbitrary waveform synthesis with multilevel pulse biasing. IEEE Trans. Appl. Supercond. **27**(3), 1301707 (2017)

94. Flowers-Jacobs, N.E., Rüfenacht, A., Fox, A.E., et al.: Three volt pulse-driven Josephson arbitrary waveform synthesizer. CPEM 2018 digest (to be accessible online via IEEE Xplore) (2018)
95. Rüfenacht, A., Flowers-Jacobs, N.E., Fox, A.E., et al.: DC comparison of a programmable Josephson voltage standard and a Josephson arbitrary waveform synthesizer. CPEM 2018 digest (to be accessible online via IEEE Xplore) (2018)
96. Gallop, J., Piquemal, F.: SQUIDs for standards and metrology. In: Clarke, J., Braginski, A.I. (eds.) The SQUID Handbook, vol. 2. Wiley (2006). ISBN-13: 978-3-527-40408-7; ISBN-10: 3-527-40408-2
97. Gallop, J., Hao, L.: Applications: Other devices—metrology. In: Cardwell, D., Larbalestier, D. (eds.) Handbook of Superconducting Materials. CRC Press (2019). ISBN-13: 978-1439817308, ISBN-10: 1439817308
98. Przybysz, J.X., Miller, D.L., Hannes Toepfer, H., et al.: Superconductor digital electronics. In: Seidel, P. (ed.) Applied Superconductivity: Handbook on Devices and Applications. Wiley (2015). ISBN: 978-3-527-41209-9
99. Buck, D.A.: The cryotron—a superconductive computer component. Proc. IRE **44**(4), 482–493 (1956). https://doi.org/10.1109/JRPROC.1956.274927
100. Bremer, J.: The invention of superconducting integrated circuit. IEEE History Center Newslett. **75**, 6–7 (2007)
101. Matisoo, J.: The tunneling cryotron—a superconductive logic element based on electron tunneling. Proc. IEEE **55**(2), 172–180 (1967). https://doi.org/10.1109/PROC.1967.5436
102. Hasuo, S.: Josephson microprocessors. In: Weinstock, H. (ed.) SQUID Sensors: Fundamentals, Fabrication and Application, p. 329. Kluwer Acad. Publ (1996). NATO ASI Ser. E-Appl. Sci
103. Likharev, K.K., Mukhanov, O.A., Semenov, V.K.: Resistive single flux quantum logic for the Josephson junction technology. In: Hahlbohm, H.D., Lübbig, H. (eds.) SQUID '85: Superconducting Quantum Interference Devices and Their Applications, pp. 1103–1108. W. de Gruyter Pbl (1985)
104. Likharev, K.K., Semenov, V.K.: RSFQ logic/memory family: A new Josephson-junction technology for sub-terahertz clock-frequency digital systems. IEEE Trans. Appl. Supercond. **1**, 3–28 (1991)
105. Mukhanov, O.A., Kirichenko, D., Vernik, I., et al.: Superconductor digital-RF receiver systems. IEICE Trans. Electron **E91-C**, 306–317 (2008)
106. Mukhanov, O.A.: Digital electronics. In: Cardwell, D., Larbalestier, D. (eds.) Handbook of Superconducting Materials. CRC Press (2019). ISBN-13: 978-1439817308, ISBN-10: 1439817308
107. Cavin, IIIR.K., Lugli, P., Zhirnov, V.V.: Science and engineering beyond Moore's Law. Proc. IEEE **100**, 1720–1749 (2012)
108. Holmes, D.S., Ripple, A.L., Manheimer, M.A.: Energy-efficient superconducting computing—power budgets and requirements. IEEE Trans. Appl. Supercond. **23**, 1701610 (2013)
109. Manheimer, M.A.: Cryogenic computing complexity program: phase 1: introduction. IEEE Trans. Appl. Supercond. **25**, 1301704 (2015)
110. Kirichenko, D.E., Sarwana, S., Kirichenko, A.F.: Zero static power dissipation biasing of RSFQ circuits. IEEE Trans. Appl. Supercond. **21**, 776–779 (2011)
111. Herr, Q.P., Herr, A., Oberg, O.T., Ioannidis, A.G.: Ultra-low-power superconductor logic. J. Appl. Phys. **109**, 103903 (2011)
112. Hosoya, M., Hioe. W., Casas, J., et al.: Quantum flux parametron: a single quantum flux device for Josephson supercomputer. IEEE Trans. Appl. Supercond. **1**(2), 77–89 (1991)
113. Takeuchi, N., Ozawa, D., Yamanashi, Y., Yoshikawa, N.Y.: Adiabatic quantum flux parametron as an ultra-low-power logic device. Supercond. Sci. Technol. **26**, 035010 (2013)
114. Landauer, R.: Irreversibility and heat generation in the computing process. IBM J. Res. Devel. **5**, 183–191 (1961)
115. Fang, K., Takeuchi, N., Ando, T., et al.: Multi-excitation AQFP. J. Appl. Phys. **121**, 143901 (2017)
116. Nagasawa, S., Numata, H., Hashimoto, Y., Tahara, S.: High-frequency clock operation of Josephson 256-word x 16-bit RAMs. IEEE Trans. Appl. Supercond. **9**, 3708–3713 (1999)
117. Van Duzer, T., Zheng, L., Whiteley, S., et al.: 64-kb hybrid Josephson-CMOS 4 Kelvin RAM with 400 ps access time and 12 mW read power. IEEE Trans. Appl. Supercond **23**, 1700504 (2013)
118. Baek, B., Rippard, W., Benz, S., et al.: Hybrid superconducting-magnetic memory device using competing order parameters. Nat. Comm. **5**, 4888 (2014)
119. Goldobin, E., Sickenger, H., Weides, M., et al.: Memory cell based on a phi Josephson junction. Appl. Phys. Lett. **102**, 242602 (2013)
120. Niedzielski, B., Gingrich, E., Loloee, R., et al.: S/F/S Josephson junctions with single-domain ferromagnets for memory applications. Supercond. Sci. Technol. **28**, 085012(2015) (2015)
121. Vernik, I., Bol'ginov, V., Bakurskiy, S., et al.: Magnetic Josephson junctions with superconducting interlayer for cryogenic memory. IEEE Trans. Appl. Supercond. **23**, 1701208 (2013)
122. Gingrich, E., Niedzielski, B., Glick, J., et al.: Controllable 0–π Josephson junctions containing a ferromagnetic spin valve. Nat. Phys. **12**, 564–567 (2016)
123. Glick, J.A., Edwards, S., Korucu, D., et al.: Spin triplet supercurrent in JJs containing a synthetic antiferromagnet with perpendicular magnetic anisotropy. arXiv:1710.07247v1 [cond.mat.supr-con] (2017)
124. Clarke, J., Wilhelm, F.K.: Superconducting quantum bits. Nature **453**, 10131 (2008)
125. Devoret, M.H., Walraff, A., Martinis, J.M.: Superconducting qubits: A short review. arXiv:cond-mat/0411174 (2008)
126. Siddiqi, I.: Superconducting qubits: poised for computing? Supercond. Sci. Technol. **24**, 091002 (2011)
127. Mooij, J.E.: Qubits. In: Rogalla, H., Kes, P.H. (eds.) 100 Years of Superconductivity, pp. 375–388. CRC Press (2011)
128. Bouchiat, V., Vion, D., Joyez, P., et al.: Quantum coherence with a single Cooper pair. Phys. Scr. **T76**, 165–170 (1998)
129. Nakamura, Y., Pashkin, Y.u.A., Tsai, J.S.: Coherent control of macroscopic quantum states in a single-Cooper-pair box. Nature **298**, 786–788 (1999)
130. IBM Online Quantum Experience (IBM Q): https://quantumexperience.ng.bluemix.net/qx/experience
131. Boixo, S., Isakov, S.V., Smelyanskiy, V.N., et al.: Characterizing quantum supremacy in near-term devices. Nat. Phys. **14**, 595–600 (2018)
132. Blais, A., Huang, R.-S., Wallraff, A., et al.: Cavity quantum electrodynamics for superconducting electrical circuits: an architecture for quantum computation. Phys. Rev. A **69**, 06320 (2004)
133. Koch. J., Yu, T.M., Gambetta, J., et al.: Charge-insensitive qubit design derived from the Cooper pair box. Phys. Rev. A **76**, 042319 (2007)
134. Chen, Y., Neill, C., Roushan, P., et al.: Qubit architecture with high coherence and fast tunable coupling. Phys. Rev. Lett. **113**, 220502 (2014)
135. Chow, J.M., Córcoles, A.D., Gambetta, J.M., et al.: Simple all-microwave entangling gate for fixed frequency supeconducting qubits. Phys. Rev. Lett. **107**, 080502 (2011)
136. Nayak, C.h., Simon, S.H., Stern, A., et al.: Non-Abelian anyons and topological quantum computation. Revs. Mod. Phys. **80**, 1083–115 (2008)

137. Kitaev, A.Y.: Unpaired Majorana fermions in quantum wires. Phys. Uspekhi **44**, 131–136 (2001)
138. Lutchyn, R.M., Sau, J.D., Das Sarma, S.: Majorana fermions and a topological phase transition in semiconductor-superconductor heterostructures. Phys. Rev. Lett. **105**, 077001 (2010)
139. Oreg, Y., Refael, G., von Oppen, F.: Helical liquids and Majorana bound states in quantum wires. Phys. Rev. Lett. **105**, 177002 (2010)
140. Zhang, H., Liu, Ch.-X., Gazibegovic, S., et al.: Quantized Majorana conductance. Nature **556**, 26142 (2018)
141. Wiedenmann, J., Bocquillon, E., Deacon, R.S., et al.: 4π-periodic Josephson supercurrent in HgTe-based topological Josephson junctions. Nat. Comm. **7**, 10303 (2016)
142. Schüffelgen, P., Rosenbach, D., Li, C., et al.: Boosting transparency in topological Josephson junctions via stencil lithography. arXiv:1711.01665 (2017)
143. Karzig, T., Knapp, C.h., Lutchyn, R.M., et al.: Scalable designs for quasiparticle-poisoning-protected topological computation with Majorana zero modes. Phys. Rev. B **95**, 235305 (2017)
144. Rønnow, T.F., Wang, Z., Job, J., et al.: Defining and detecting quantum speedup. arXiv:1401.2910v1 (2014)
145. Denchev, V.S., Boixo, S., Isakov, S.V., et al.: What is the computational value of finite-range tunneling? Phys. Rev. X **6**, 031015 (2016)
146. D-Wave: https://www.dwavesys.com/resources/publications